and DEM, in order to clarify the mechanism of induction observed in the present study.

In conclusion, we have detected dynamic changes in the Nrf2 system *in vivo*, associated with 2 discrete chemical agents. These changes are not dependent on a toxic effect of these agents on the liver but are associated with changes in the hepatic level of reduced GSH and the presence of a chemical species with the potential for covalent modification, with the likely consequent oxidative alterations in cell regulatory and sensor proteins. The induction profile seen with Nrf2-regulated genes following acetaminophen treatment, whereby induction was impaired at very high doses despite the linear increase in nuclear Nrf2, may have therapeutic consequences for the targeting of Nrf2 in chemoprotection. The strategic induction of Nrf2 to boost cellular defense mechanisms may alone provide insufficient protection against some forms of chemical stress without the concomitant maintenance of related cellular functions.

Acknowledgment: The authors thank Sylvia Newby and Phil Roberts for technical assistance and Dr. Nicola Hanrahan for assistance with the glutathione assay.

References

1. Prestera T, Zhang Y, Spencer SR, Wilczak CA, Talalay P. The electrophile counterattack response: protection against neoplasia and toxicity. Adv Enzyme Regul 1993;33:281–296.
2. Hayes JD, McMahon M. Molecular basis for the contribution of the antioxidant responsive element to cancer chemoprevention. Cancer Lett 2001;174:103–113.
3. Friling RS, Bergelson S, Daniel V. Two adjacent AP-1-like binding sites form the electrophile-responsive element of the murine glutathione S-transferase Ya subunit gene. Proc Natl Acad Sci USA 1992;89:668–672.
4. Jaiswal AK. Antioxidant response element. Biochem Pharmacol 1994;48: 439–444.
5. Rushmore TH, Pickett CB. Transcriptional regulation of the rat glutathione S-transferase Ya subunit gene. Characterization of a xenobiotic-responsive element controlling inducible expression by phenolic antioxidants. J Biol Chem 1990;265:14648–14653.
6. Rushmore TH, Morton MR, Pickett CB. The antioxidant responsive element. Activation by oxidative stress and identification of the DNA consensus sequence required for functional activity. J Biol Chem 1991;266: 11632–11639.
7. Andrews NC, Erdjument-Bromage H, Davidson MB, Tempst P, Orkin SH. Erythroid transcription factor NF-E2 is a haematopoietic-specific basic-leucine zipper protein. Nature 1993;362:722–728.
8. Venugopal R, Jaiswal AK. Nrf1 and Nrf2 positively and c-Fos and Fra1 negatively regulate the human antioxidant response element-mediated expression of NAD(P)H:quinone oxidoreductase1 gene. Proc Natl Acad Sci USA 1996;93:14960–14965.
9. Wild AC, Moinova HR, Mulcahy RT. Regulation of gamma-glutamylcysteine synthetase subunit gene expression by the transcription factor Nrf2. J Biol Chem 1999;274:33627–33636.
10. Alam J, Stewart D, Touchard C, Boinapally S, Choi AM, Cook JL. Nrf2, a Cap'n'Collar transcription factor, regulates induction of the heme oxygenase-1 gene. J Biol Chem 1999;274:26071–26078.
11. Jeyapaul J, Jaiswal AK. Nrf2 and c-Jun regulation of antioxidant response element (ARE)-mediated expression and induction of gamma-glutamylcysteine synthetase heavy subunit gene. Biochem Pharmacol 2000;59:1433–1439.
12. Chanas SA, Jiang Q, McMahon M, McWalter GK, McLellan LI, Elcombe CR, et al. Loss of the Nrf2 transcription factor causes a marked reduction in constitutive and inducible expression of the glutathione S-transferase Gsta1, Gsta2, Gstm1, Gstm2, Gstm3 and Gstm4 genes in the livers of male and female mice. Biochem J 2002;365:405–416.
13. Chan K, Kan YW. Nrf2 is essential for protection against acute pulmonary injury in mice. Proc Natl Acad Sci USA 1999;96:12731–12736.
14. Enomoto A, Itoh K, Nagayoshi E, Haruta J, Kimura T, O'Connor T, et al. High sensitivity of Nrf2 knockout mice to acetaminophen hepatotoxicity associated with decreased expression of ARE-regulated drug metabolizing enzymes and antioxidant genes. Toxicol Sci 2001;59:169–177.
15. McMahon M, Itoh K, Yamamoto M, Chanas SA, Henderson CJ, McLellan LI, et al. The Cap'n'Collar basic leucine zipper transcription factor Nrf2 (NF-E2 p45-related factor 2) controls both constitutive and inducible expression of intestinal detoxification and glutathione biosynthetic enzymes. Cancer Res 2001;61:3299–3307.
16. Kong AN, Owuor E, Yu R, Hebbar V, Chen C, Hu R, et al. Induction of xenobiotic enzymes by the map kinase pathway and the antioxidant or electrophile response element (ARE/EpRE). Drug Metab Rev 2001;33: 255–271.
17. Itoh K, Wakabayashi N, Katoh Y, Ishii T, Igarashi K, Engel JD, et al. Keap1 represses nuclear activation of antioxidant responsive elements by Nrf2 through binding to the amino-terminal Neh2 domain. Genes Dev 1999;13:76–86.
18. Wakabayashi N, Itoh K, Wakabayashi J, Motohashi H, Noda S, Takahashi S, et al. Keap1-null mutation leads to postnaral lethality due to constitutive Nrf2 activation. Nat Genet 2003;35:238–245.
19. Itoh K, Wakabayashi N, Katoh Y, Ishii T, O'Connor T, Yamamoto M. Keap1 regulates both cytoplasmic-nuclear shuttling and degradation of Nrf2 in response to electrophiles. Genes Cells 2003;8:379–391.
20. Nguyen T, Sherratt PJ, Huang HC, Yang CS, Pickett CB. Increased protein stability as a mechanism that enhances Nrf2-mediated transcriptional activation of the antioxidant response element. Degradation of Nrf2 by the 26 S proteasome. J Biol Chem 2003;278:4536–4541.
21. McMahon M, Itoh K, Yamamoto M, Hayes JD. Keap1-dependent proteasomal degradation of transcription factor Nrf2 contributes to the negative regulation of antioxidant response element-driven gene expression. J Biol Chem 2003;278:21592–21600.
22. Dinkova-Kostova AT, Massiah MA, Bozak RE, Hicks RJ, Talalay P. Potency of Michael reaction acceptors as inducers of enzymes that protect against carcinogenesis depends on their reactivity with sulfhydryl groups. Proc Natl Acad Sci USA 2001;98:3404–3409.
23. Ostapowicz G, Fontana RJ, Schiodt FV, Larson A, Davern TJ, Han SH, et al. Results of a prospective study of acute liver failure at 17 tertiary care centers in the United States. Ann Intern Med 2002;137:947–954.
24. Fagan E, Wannan G. Reducing paracetamol overdoses. Br Med J 1996; 313:1417–1418.
25. Pierce RH, Franklin CC, Campbell JS, Tonge RP, Chen W, Fausto N, et al. Cell culture model for acetaminophen-induced hepatocyte death in vivo. Biochem Pharmacol 2002;64:413–424.
26. Lee SS, Buters JT, Pineau T, Fernandez-Salguero P, Gonzalez FJ. Role of CYP2E1 in the hepatotoxicity of acetaminophen. J Biol Chem 1996;271: 12063–12067.
27. Zaher H, Buters JT, Ward JM, Bruno MK, Lucas AM, Stern ST, et al. Protection against acetaminophen toxicity in CYP1A2 and CYP2E1 double-null mice. Toxicol Appl Pharmacol 1998;152:193–199.
28. Potter WZ, Thorgeirsson SS, Jollow DJ, Mitchell JR. Acetaminophen-induced hepatic necrosis. V. Correlation of hepatic necrosis, covalent binding and glutathione depletion in hamsters. Pharmacology 1974;12:129–143.
29. Muldrew KL, James LP, Coop L, McCullough SS, Hendrickson HP, Hinson JA, et al. Determination of acetaminophen-protein adducts in mouse liver and serum and human serum after hepatotoxic doses of acetaminophen using high-performance liquid chromatography with electrochemical detection. Drug Metab Dispos 2002;30:446–451.

30. Harman AW. The effectiveness of antioxidants in reducing paracetamol-induced damage subsequent to paracetamol activation. Res Commun Chem Pathol Pharmacol 1985;49:215–228.
31. Cohen SD, Hoivik DJ, Khairallah EA. In: Plaa GL, Hewitt WR, eds. Toxicology of the Liver. Vol. 1. 2nd ed. Washington D.C.: Taylor & Francis; 1998; 159–186.
32. Jaeschke H, Knight TR, Bajt ML. The role of oxidant stress and reactive nitrogen species in acetaminophen hepatotoxicity. Toxicol Lett 2003;144: 279–288.
33. Chan K, Han XD, Kan YW. An important function of Nrf2 in combating oxidative stress: detoxification of acetaminophen. Proc Natl Acad Sci USA 2001;98:4611–4616.
34. Kitteringham NR, Powell H, Clement YN, Dodd CC, Tettey JN, Pirmohamed M, et al. Hepatocellular response to chemical stress in CD-1 mice: induction of early genes and gamma-glutamylcysteine synthetase. HEPATOLOGY 2000;32:321–333.
35. Vandeputte C, Guizon I, Genestie-Denis I, Vannier B, Lorenzon G. A microtiter plate assay for total glutathione and glutathione disulfide contents in cultured/isolated cells: performance study of a new miniaturized protocol. Cell Biol Toxicol 1994;10:415–421.
36. Dignam JD, Lebovitz RM, Roeder RG. Accurate transcription initiation by RNA polymerase II in a soluble extract from isolated mammalian nuclei. Nucleic Acids Res 1983;11:1475–1489.
37. Israel N, Gougerot-Pocidalo MA, Aillet F, Virelizier JL. Redox status of cells influences constitutive or induced NF-kappa B translocation and HIV long terminal repeat activity in human T and monocytic cell lines. J Immunol 1992;149:3386–3393.
38. Nguyen T, Sherratt PJ, Pickett CB. Regulatory mechanisms controlling gene expression mediated by the antioxidant response element. Annu Rev Pharmacol Toxicol 2003;43:233–260.
39. Liu RM, Hu H, Robison TW, Forman HJ. Differential enhancement of gamma-glutamyl transpeptidase and gamma-glutamylcysteine synthetase by tert-butylhydroquinone in rat lung epithelial L2 cells. Am J Respir Cell Mol Biol 1996;14:186–191.
40. Hayes JD, Chanas SA, Henderson CJ, McMahon M, Sun C, Moffat GJ, et al. The Nrf2 transcription factor contributes both to the basal expression of glutathione S-transferases in mouse liver and to their induction by the chemopreventive synthetic antioxidants, butylated hydroxyanisole and ethoxyquin. Biochem Soc Trans 2000;28:33–41.
41. Sekhar KR, Long M, Long J, Xu ZQ, Summar ML, Freeman ML. Alteration of transcriptional and post-transcriptional expression of gamma-glutamylcysteine synthetase by diethyl maleate. Radiat Res 1997;147:592–597.
42. Kwak MK, Itoh K, Yamamoto M, Sutter TR, Kensler TW. Role of transcription factor Nrf2 in the induction of hepatic phase 2 and antioxidative enzymes in vivo by the cancer chemoprotective agent, 3H-1, 2-dimethiole-3-thione. Mol Med 2001;7:135–145.
43. Ramos-Gomez M, Kwak MK, Dolan PM, Itoh K, Yamamoto M, Talalay P, et al. Sensitivity to carcinogenesis is increased and chemoprotective efficacy of enzyme inducers is lost in nrf2 transcription factor-deficient mice. Proc Natl Acad Sci USA 2001;98:3410–3415.
44. Mitchell JR, Jollow DJ, Potter WZ, Gillette JR, Brodie BB. Acetaminophen-induced hepatic necrosis. IV. Protective role of glutathione. J Pharmacol Exp Ther 1973;187:211–217.
45. Qiu Y, Benet LZ, Burlingame AL. Identification of the hepatic protein targets of reactive metabolites of acetaminophen in vivo in mice using two-dimensional gel electrophoresis and mass spectrometry. J Biol Chem 1998;273:17940–17953.
46. Dinkova-Kostova AT, Holtzclaw WD, Cole RN, Itoh K, Wakabayashi N, Katoh Y, et al. Direct evidence that sulfhydryl groups of Keap1 are the sensors regulating induction of phase 2 enzymes that protect against carcinogens and oxidants. Proc Natl Acad Sci USA 2002;99:11908–11913.
47. Sekhar KR, Crooks PA, Sonar VN, Friedman DB, Chan JY, Meredith MJ, et al. NADPH Oxidase Activity Is Essential for Keap1/Nrf2-mediated Induction of GCLC in Response to 2-Indol-3-yl-methylenequinuclidin-3-ols. Cancer Res 2003;63:5636–5645.
48. Shibata T, Kondo M, Osawa T, Shibata N, Kobayashi M, Uchida K. 15-deoxy-delta 12,14-prostaglandin J2. A prostaglandin D2 metabolite generated during inflammatory processes. J Biol Chem 2002;277:10459–10466.
49. Shibata T, Yamada T, Ishii T, Kumazawa S, Nakamura H, Masutani H, et al. Thioredoxin as a molecular target of cyclopentenone prostaglandins. J Biol Chem 2003;278:26046–26054.
50. Levonen AL, Landar A, Ramachandran A, Ceaser EK, Dickinson DA, Zanoni G, et al. Cellular mechanisms of redox cell signaling: role of cysteine modification in controlling antioxidant defenses in response to electrophilic lipid oxidation products. Biochem J 2004;378:373–382.

Nrf2 deficiency causes tooth decolourization due to iron transport disorder in enamel organ

Toru Yanagawa[1], Ken Itoh[1,2], Junya Uwayama[1], Yasuaki Shibata[4], Akira Yamaguchi[4], Tsuneyoshi Sano[5], Tetsuro Ishii[1], Hiroshi Yoshida[1] and Masayuki Yamamoto[1,2,3,*]

[1]*Graduate School of Comprehensive Human Sciences,* [2]*JST-ERATO Environmental Response Project,* [3]*Centre for Tsukuba Advanced Research Alliance, University of Tsukuba, 1-1-1 Tennoudai, Tsukuba 305-8577, Japan*

[4]*Division of Oral Pathology and Bone Metabolism, Department of Developmental and Reconstructive Medicine, Nagasaki University Graduate School of Biomedical Sciences, 1-7-1 Sakamoto, Nagasaki, 852-8588, Japan*

[5]*Department of Oral Anatomy, Showa University School of Dentistry, 1-5-8 Hatanodai, Shinagawa-ku, Tokyo 142-8585, Japan*

Rodents have brownish-yellow incisors whose colour represents their iron content. Iron is deposited into the mature enamel by ameloblasts that outline enamel surface of the teeth. Nrf2 is a basic region-leucine zipper type transcription factor that regulates expression of a range of cytoprotective genes in response to oxidative and xenobiotic stresses. We found that genetically engineered Nrf2-deficient mice show decolourization of the incisors. While incisors of wild-type mice were brownish yellow, incisors of Nrf2-deficient mice were greyish white in colour. Micro X-ray imaging analysis revealed that the iron content in Nrf2-deficient mouse incisors were significantly decreased compared to that of wild-type mice. We found that iron was aberrantly deposited in the papillary layer cells of enamel organ in Nrf2-deficient mouse, suggesting that the iron transport from blood vessels to ameloblasts was disturbed. We also found that ameloblasts of Nrf2-null mouse show degenerative atrophy at the late maturation stage, which gives rise to the loss of iron deposition to the surface of mature enamel. Our results thus demonstrate that the enamel organ of Nrf2-deficient mouse has a reduced iron transport capacity, which results in both the enamel cell degeneration and disturbance of iron deposition on to the enamel surface.

Introduction

The brownish yellow colour of the rodent incisors is due to iron deposition in the enamel surface layer (Halse 1973, 1974; Halse & Selvig 1974; Kallenbach 1970). In the enamel organ of rodents, where the tooth develops, a layer of cells that outline the enamel surface called ameloblasts contain the entire sequence of cell development stages. From the apical end toward the incisal end these stages are classified regionally into presecretory, secretory, transition, and maturation stages. Secretory ameloblasts produce enamel matrix proteins, whereas ameloblasts at the maturation stage act to incorporate iron and deposit it into the surface of the mature enamel, in addition to their fundamental roles in enamel formation.

Communicated by: Shunsuke Ishii
**Correspondence*: E-mail: masi@tara.tsukuba.ac.jp

DOI: 10.1111/j.1365-2443.2004.00753.x

In this unique iron transport system, ferritin functions as a transient iron reservoir in the cell, sequestering iron into the cytoplasmic granules (Karim & Warshawsky 1984). This particle first appears free in the cytoplasm, and then gradually becomes confined to the membrane bound ferritin-containing vesicles with the progression of cell developmental stages. Finally, the iron is secreted from ameloblasts into the enamel surface at the end of maturation, presumably through the process of lysosomal digestion of ferritin (Takano & Ozawa 1981).

Iron is critically involved in a wide variety of cellular events ranging from DNA synthesis to cellular respiration (Cammack *et al.* 1990). However, at the same time, free iron generates highly reactive oxygen species via Fenton chemistry and causes an oxidative stress to cells (Linn 1998). Thus, the cellular iron metabolism should be strictly regulated in the presence of various transport and storage proteins (McCord 1998).

Nrf2 belongs to the CNC transcription factor family which share a characteristic basic domain first identified in the Drosophila cap'n'collar (CNC) protein (Itoh *et al.* 1995; Mohler *et al.* 1991). Nrf2 is essential for the coordinate transcriptional induction of phase II enzymes and anti-oxidant genes via anti-oxidant responsive element (ARE) (Itoh *et al.* 1997; Ishii *et al.* 2000). Furthermore, Nrf2 constitutes a crucial cellular sensor for oxidative stress together with its cytoplasmic repressor Keap1, and mediates a key step in the signalling pathway by a novel Nrf2 nuclear shuttling mechanism (Itoh *et al.* 1999b). Activation of Nrf2 leads to the induction of phase II enzyme and anti-oxidant stress genes in response to various stresses (Ishii *et al.* 2000; Itoh *et al.* 1999a).

Whereas Nrf2-deficient mice (*Nrf2*$^{-/-}$) grow normally and are fertile (Itoh *et al.* 1997), the mice are susceptible to various oxidative stresses including acetaminophen intoxication (Enomoto *et al.* 2001; Chan *et al.* 2001), BHT intoxication (Chan & Kan 1999), chemical carcinogenesis (Ramos-Gomez *et al.* 2001), hyperoxia (Cho *et al.* 2002), and diesel exhaust inhalation (Aoki *et al.* 2001). The *Nrf2*$^{-/-}$ mice are also susceptible to lupus-like autoimmune nephritis (Yoh *et al.* 2001). However, no apparent phenotype has yet been described (Itoh *et al.* 1997; Kuroha *et al.* 1998). In this study, we found that incisors of the *Nrf2*$^{-/-}$ mice are decolourized and become greyish white. The examination of the mechanisms leading to the decolourization in the *Nrf2*$^{-/-}$ mouse revealed that the iron transport is defective in the developing enamel organ of *Nrf2*$^{-/-}$ mice.

Results

Decolourization of the maxillary incisors of *Nrf2*$^{-/-}$ mice

In an attempt to find subtle anatomical changes in the germ line *Nrf2*$^{-/-}$ mice (Itoh *et al.* 1997), we noticed that the incisors of *Nrf2*$^{-/-}$ mice are always greyish white (Fig. 1B), while in contrast, incisors of wild-type and heterozygous mutant (*Nrf2*$^{+/-}$) mice are always brownish yellow (Fig. 1A). In order to examine the decolourization phenotype in more detail, we mated *Nrf2*$^{+/-}$ male with *Nrf2*$^{+/-}$ female mice and examined 50 mice for the relationship between *Nrf2* genotype and the incidence of decolourization by macroscopic examination. Fourteen mice had greyish-white incisors and all of them were homozygous for the *Nrf2* germ line mutation. On the contrary, of the 36 mice with brownish yellow incisors, 26 were *Nrf2* heterozygous and 10 were wild-type. Thus, the penetration of decolourization phenotype in *Nrf2*$^{-/-}$ mice was 100% ($P < 0.001$).

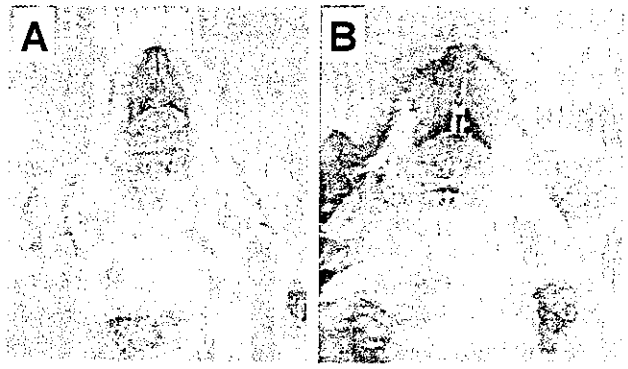

Figure 1 Incisors of *Nrf2*$^{-/-}$ mice are decolourized. The incisors of wild-type mouse show the normal brownish-yellow colour (A), whereas the incisors of *Nrf2*$^{-/-}$ mice have greyish white colour (B).

Iron content in enamel surface was specifically decreased in *Nrf2*$^{-/-}$ mice

Scanning electron microscopic analysis detected no significant structural differences in the tooth surface between wild-type (Fig. 2A) and *Nrf2*$^{-/-}$ mice (Fig. 2D). However, X-ray microanalysis revealed an apparent difference in the iron content on the enamel surfaces between the *Nrf2*$^{-/-}$ and wild-type mice (Table 1). A dot-map image analysis revealed the remarkable decrease of iron content in the enamel surface of *Nrf2*$^{-/-}$ mouse incisors (Fig. 2F) compared to those of wild-type mice (Fig. 2C). Calcium content was within comparable range between wild-type (Fig. 2B) and *Nrf2*$^{-/-}$ mice (Fig. 2E).

Table 1 summarizes the calcium, phosphorus and iron contents of the incisors that were quantified by X-ray microanalysis. Importantly, we found that the mean iron content (Fe% (w/w)) of the *Nrf2*$^{-/-}$ mouse enamel was less than one-tenth of that of the wild-type mouse. The decrease shows gene copy number dependence such that in the *Nrf2*$^{+/-}$ mouse incisors the mean iron content was about one half of that of the wild-type mice. In contrast, no significant difference was observed in the content of calcium and phosphorus amongst *Nrf2*$^{-/-}$, *Nrf2*$^{+/-}$ and wild-type mice. Similarly, the molar ratio (MR) as well as weight percentage ratio (WR) of calcium to potassium was unaffected. These results indicate that the iron metabolism is specifically affected in the *Nrf2*$^{-/-}$ mouse teeth.

General iron status in *Nrf2*$^{-/-}$ mice

To examine the reason why the iron metabolism of enamel organ was impaired in *Nrf2*$^{-/-}$ mice, we measured the general iron status in *Nrf2*$^{-/-}$ mice. We did not find any significant differences in haematocrit, serum iron concentration, total iron binding capacity (TIBC) and transferrin saturation (Table 2), indicating that the general iron status of *Nrf2*$^{-/-}$

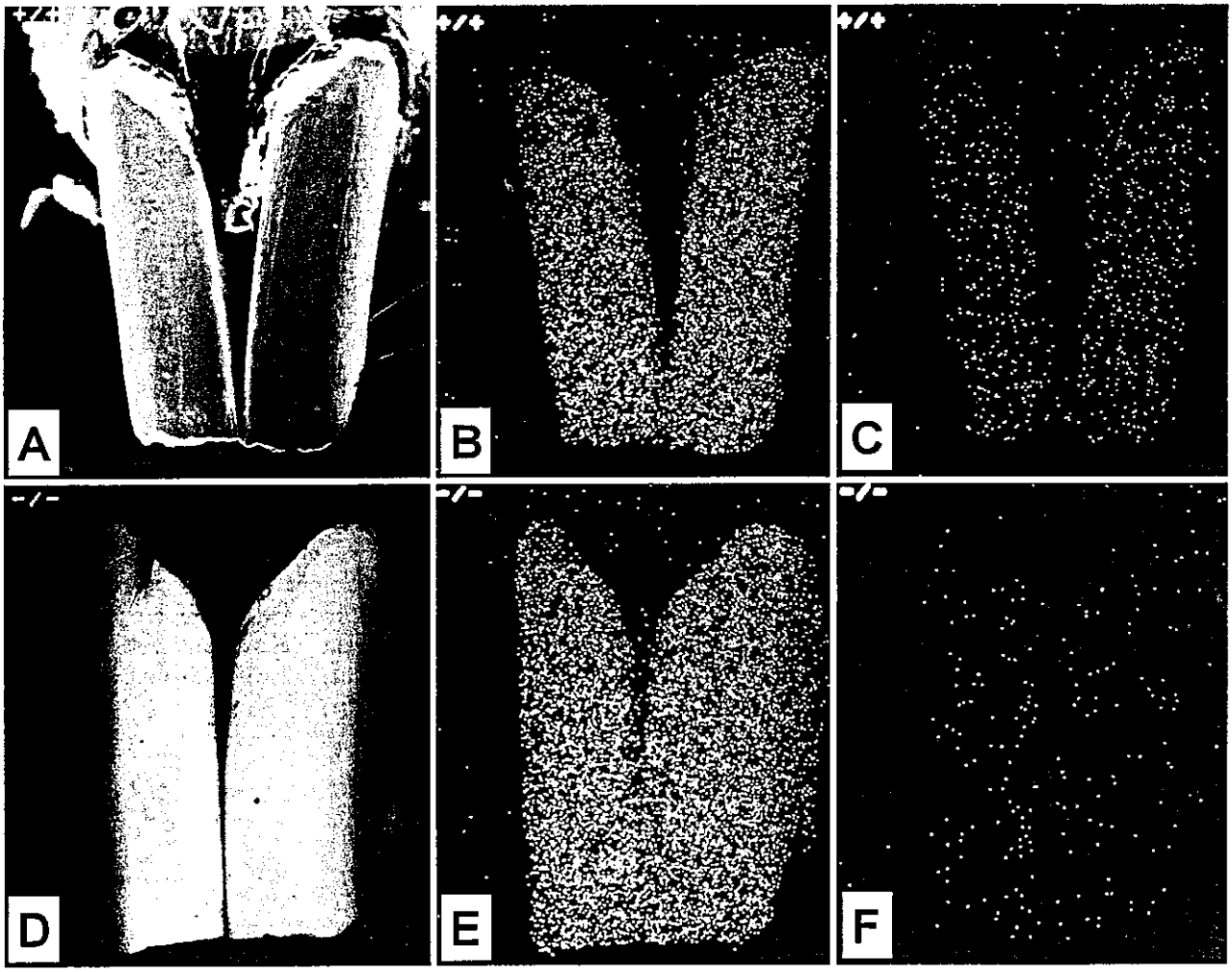

Figure 2 Scanning electron microscopic and micro X-ray analysis of the surface of the mouse incisor. (A, D) Scanning electron microscopic images of incisors of wild-type (A) and *Nrf2*$^{-/-}$ mouse (D). (B, E) Dot-map images of calcium on the surface of wild-type (B) and *Nrf2*$^{-/-}$ incisors (E) by micro X-ray analysis. (C, F) Dot-map images of iron on the surface of wild-type (C) and *Nrf2*$^{-/-}$ mouse incisors (F).

Table 1 Micro X-ray analysis of the incisors of *Nrf2*$^{-/-}$ mutant mice

	Nrf2 genotype		
	+/+	+/–	–/–
Fe percentage (w/w)	5.143 ± 0.754	2.748 ± 0.454*	0.396 ± 0.076*
Ca percentage (w/w)	36.389 ± 0.222	36.073 ± 0.039	36.161 ± 0.067
P percentage (w/w)	18.057 ± 0.091	17.808 ± 0.104	17.954 ± 0.047
Ca/P WR	2.016 ± 0.006	2.026 ± 0.011	2.015 ± 0.007
Ca/P MR	1.558 ± 0.005	1.566 ± 0.008	1.555 ± 0.007

The calcium, phosphorus, and iron contents of the enamel surface of wild-type, *Nrf2*$^{+/-}$, or *Nrf2*$^{-/-}$ incisors determined by micro X-ray analysis. The means from five incisors are presented with standard deviations. Student's *t*-test was used for the statistical analysis. *Significant difference compared with wild-type ($P < 0.001$). % (w/w), weigh percent; Ca/P WR, weight percentage ratio of calcium to phosphorus; Ca/P MR, molar ratio of calcium to phosphorus.

Table 2 General iron status of *Nrf2*$^{-/-}$ mice

	Nrf2 genotype	
	+/+	−/−
Hematocrit (%)	52.2 ± 4.9	52.7 ± 2.9
Serum iron (g/dL)	219.5 ± 40.6	271.0 ± 50.5
TIBC (g/dL)	407.8 ± 52.6	460.3 ± 71.2
Transferrin saturation (%)	54.4 ± 11.8	59.1 ± 8.7
Liver iron content (ng/mg)	55.5 ± 18.0	90.0 ± 11.7*

Hematocrit, serum iron concentration, total iron binding capacity (TIBC), transferrin saturation and liver iron content were measured in wild-type and Nrf2$^{-/-}$ mice. The means from six mice are presented with standard deviations. Mann–Whitney's *U*-test was used for the statistical analysis. *Significant difference compared with wild-type ($P < 0.01$).

mice is not affected. In contrast, non-haem iron content of liver was found to be significantly higher in *Nrf2*$^{-/-}$ mice than that in wild-type liver. The precise reason of this iron increase in the liver remains to be clarified.

Ameloblasts of *Nrf2*$^{-/-}$ mice show premature degenerative atrophy

We next examined development of ameloblasts in *Nrf2*$^{-/-}$ mouse, since it is the ameloblasts that deposit iron into the enamel surface. A histological examination with lower magnification of wild-type mouse tissues with haematoxylin and eosin staining showed slight signs of degenerative atrophy in the late maturation stage of the ameloblast development (lm, Fig. 3A). Compared to the wild-type mice, however, these changes in the *Nrf2*$^{-/-}$ mouse ameloblasts were abrupt and premature (below). We found that, while ameloblasts of *Nrf2*$^{-/-}$ mice showed very similar morphological appearance to that of the wild-type mice during the transition (t) stage and the early maturation (em) stage,

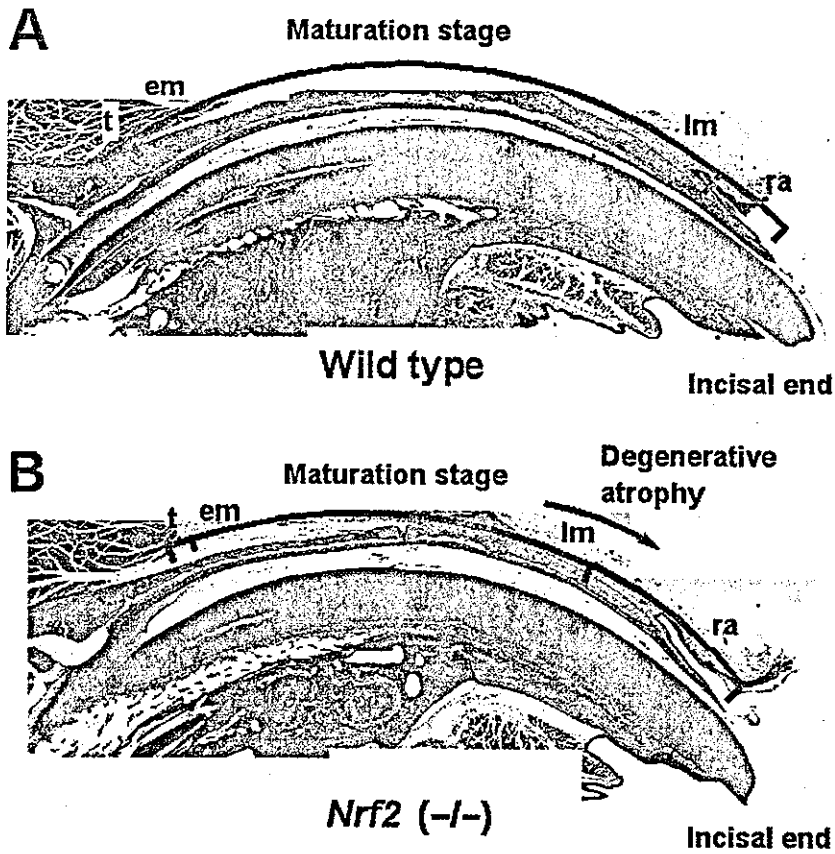

Figure 3 *Nrf2*$^{-/-}$ ameloblasts show degenerative atrophy at the late maturation stage. (A, B) Hematoxylin and eosin staining of wild-type (A) and *Nrf2*$^{-/-}$ (B) mouse enamel organs. The ameloblasts of *Nrf2*$^{-/-}$ mouse show severe premature degenerative atrophy at the late maturation stage (40 × original magnification). Abbreviations are: t, transition stage; em, early maturation stage; lm, late maturation stage; ra, region of reduced ameloblasts.

ameloblasts of *Nrf2*$^{-/-}$ mice suffered severely from premature degenerative atrophy at the late maturation stage (Fig. 3B; green arrow). The late maturation stage is the time when iron is excreted from ameloblasts to the enamel surface. At higher magnification, cell heights of ameloblasts gradually reduced from the early maturation stage to the late maturation stage in wild-type ameloblasts. At the stages of reduced ameloblasts, they were changed to atrophic flat squamous cells on the most incisal side. In agreement with the observations with the lower magnification sections (Fig. 3B), *Nrf2*$^{-/-}$ mice ameloblasts showed similar morphological appearance to the wild-type ameloblasts during the transition stage (Fig. 4A,C). However, the *Nrf2*$^{-/-}$ ameloblasts suffered from premature degenerative changes at the late maturation stage (Fig. 4D; compare with those in the wild-type mouse, Fig. 4B) and the flat squamous epithelia largely disappeared in the mutant mouse tissues (data not shown). These results thus demonstrate that the normal differentiation of ameloblasts are severely disturbed at the late maturation stage in the *Nrf2*$^{-/-}$ mice.

Iron transport is defective in *Nrf2*$^{-/-}$ mice

To examine whether the incomplete differentiation affects the ameloblasts function, iron metabolism during the ameloblast development was examined in *Nrf2*$^{-/-}$ mice. We carried out Berlin blue staining of wild-type and *Nrf2*$^{-/-}$ mouse incisors (Fig. 4, panels E–H). In the wild-type mouse incisors, positive staining of Berlin blue, which indicates the accumulation of iron, was detected in the ameloblast cytosol during the transition stage and early maturation stage (Fig. 4E). The accumulation of iron was then shifted to the plasma membrane on the enamel side at the late maturation stage, reflecting the iron excretion process into the enamel surface at this stage (Fig. 4F). No Berlin blue-positive staining was detected at the reduced ameloblast stage (data not shown). In the *Nrf2*$^{-/-}$ enamel organ, iron was detected both in the papillary layer cells and ameloblasts during the transition and early maturation stages, and the iron accumulation in the ameloblast cytosol was markedly decreased (Fig. 4G). This may be due to defect of the iron transport from blood vessels to the ameloblasts. We also found that the aberrant iron deposition overlapping with the degenerated cells (Fig. 4H), suggesting that the abnormal accumulation of iron might provoke, at least in part, the degeneration of papillary cells and ameloblasts of *Nrf2*$^{-/-}$ enamel organ.

Ferritin expression was decreased in *Nrf2*$^{-/-}$ papillary layer cells

Since ferritin is known to play an important role in the cellular iron metabolism, we next examined the expression of ferritin by immunohistochemical and *in situ* hybridization analyses. Ferritin heavy chain mRNA was expressed exclusively in the ameloblasts during transition and early maturation stages. The *Nrf2*$^{-/-}$ ameloblasts show similar level expression to the wild-type ameloblasts (Fig. 5C and 5A, respectively). However, ferritin heavy chain mRNA expression was very faint or not observed in the late maturation stage and reduced ameloblast stage (data not shown) of the ameloblast development in both wild-type and *Nrf2*$^{-/-}$ mice (Fig. 5B and 5D, respectively).

We also performed immunohistochemical analysis of ferritin expression, utilizing an anti-rat liver ferritin antibody that cross-reacts with mouse ferritin (Miyazaki *et al.* 1998). The analysis revealed that the expression level of ferritin protein was comparable between ameloblasts and papillary layer cells at the transition and early maturation stages in the wild-type mouse (Fig. 5E). Importantly, however, in the *Nrf2*$^{-/-}$ mouse the expression of ferritin in the papillary layer cells was significantly reduced compared to that in the ameloblasts (Fig. 5G). Consistent with the results of *in situ* ferritin heavy chain mRNA analysis, ferritin was expressed only faintly in the more advanced stages of ameloblasts (Fig. 5F,H). These results clearly indicate that although ferritin is expressed in the ameloblasts, it is not expressed efficiently in the papillary layer cells of *Nrf2*$^{-/-}$ animals (see Discussion).

Nrf2$^{-/-}$ teeth have decreased acid resistance

To assess changes in the quality of the teeth, we first examined the Knoop hardness of the teeth. However, we could not detect significant difference between wild-type and *Nrf2*$^{-/-}$ teeth. Therefore, we next examined acid resistance of *Nrf2*$^{-/-}$ teeth. For this purpose, the teeth were exposed to 0.1 M acetate buffer at pH 4.0 and amounts of eluted calcium ion were quantified at several time points by the methylxylenol blue method. As shown in Fig. 6, the concentration of eluted calcium ion from *Nrf2*$^{-/-}$ teeth was significantly higher than that from the wild-type teeth. The initial elution velocity increased rapidly, but the elution seems to be saturated at 30 and 40 min time points in *Nrf2*$^{-/-}$ teeth. The eluted calcium level from the *Nrf2*$^{-/-}$ teeth is significantly higher than that from the wild-type teeth ($P < 0.05$: Student's *t*-test). Thus, the acid resistance of *Nrf2*$^{-/-}$ teeth was significantly decreased compared to that of the wild-type mice, suggesting that the *Nrf2*$^{-/-}$ teeth are susceptible to dental caries.

Discussion

Closer examination of the *Nrf2*$^{-/-}$ mice unveiled that the surface colour of maxillary incisors of the *Nrf2*$^{-/-}$ mice is

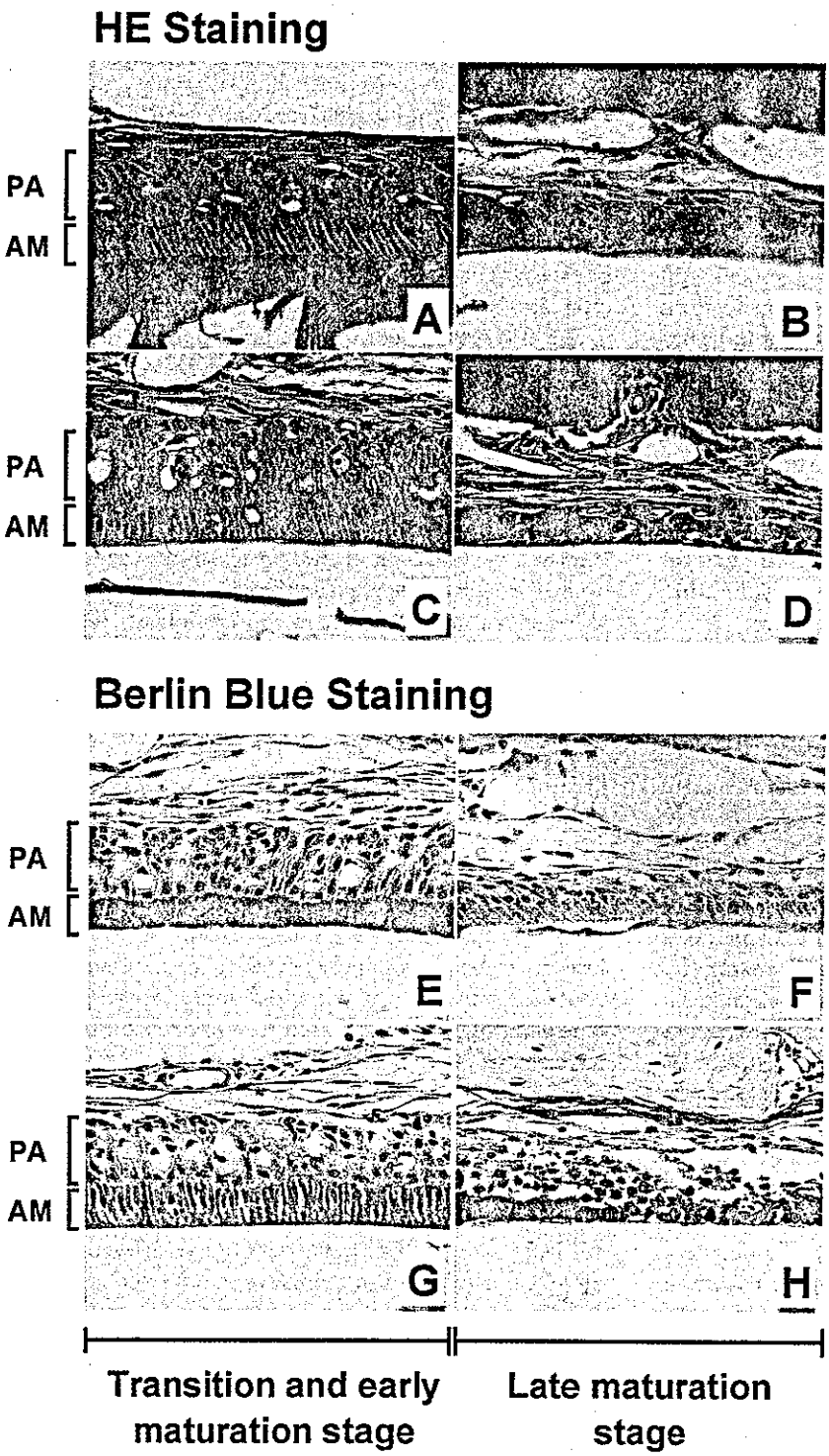

Figure 4 Defective iron transport in *Nrf2*$^{-/-}$ mouse enamel organ. (A–D) Hematoxylin and eosin staining of wild-type (A, B) and *Nrf2*$^{-/-}$ (C, D) mouse enamel organs. (E–H) Berlin blue staining of wild-type (E, F) and *Nrf2*$^{-/-}$ (G, H) mouse enamel organs. (A, C, E, G) show the transition stage, while (B, D, F, H) show the late maturation stage of ameloblast maturation. AM, ameloblasts; PA, Papillary cell layer.

greyish white, which is a marked contrast to the yellowish brown colour of the wild-type mouse incisors. Our analyses further revealed that this decolourization is due to the decrease in the iron content of the mature enamel.

The analysis of iron metabolism in the enamel organ showed that the iron transport from blood vessels to the ameloblasts was disturbed in the *Nrf2*$^{-/-}$ mouse during the ameloblast maturation stages. In the *Nrf2*$^{-/-}$ mouse,

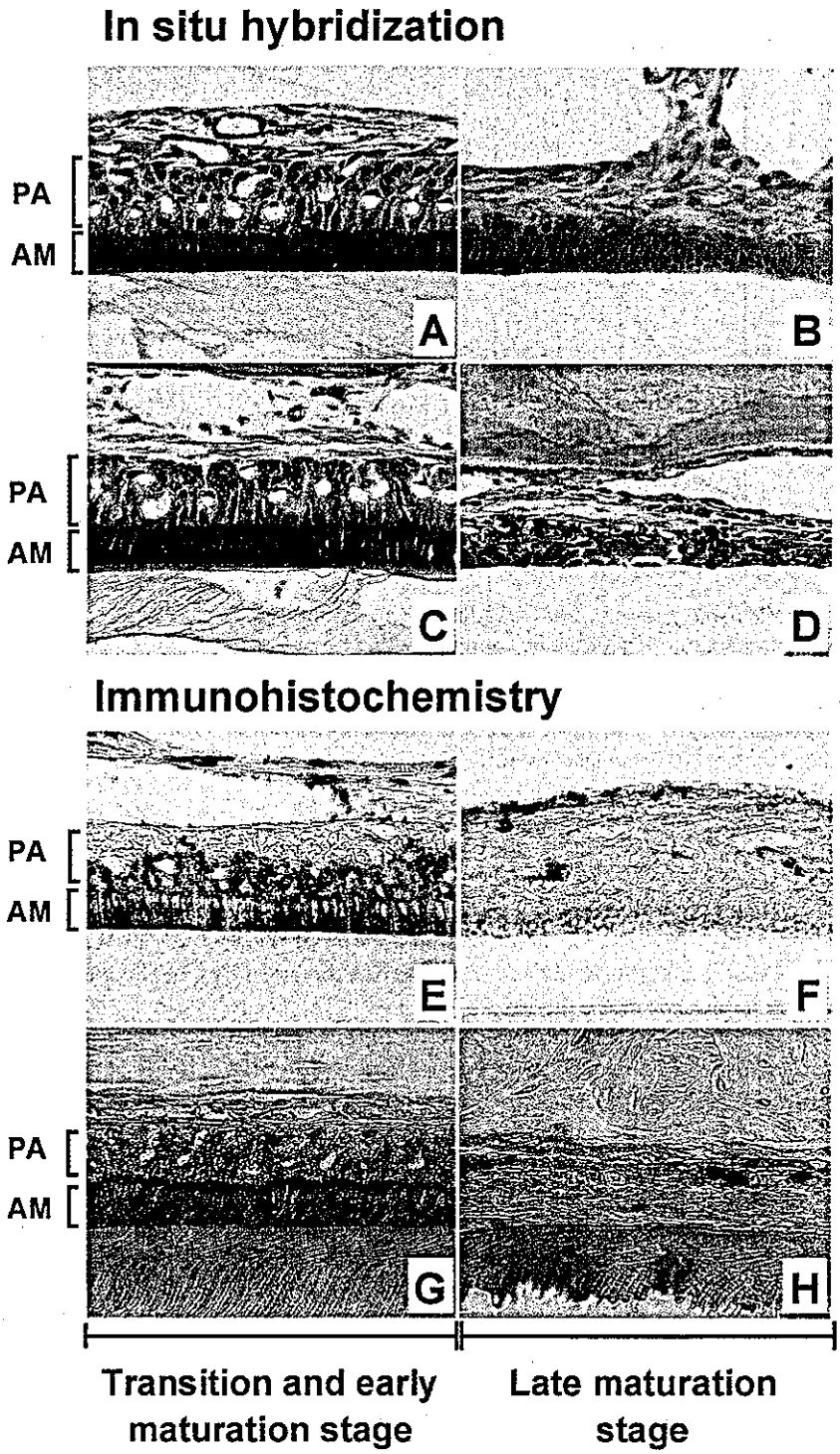

Figure 5 Expression of ferritin and ferritin heavy chain mRNA in *Nrf2*$^{-/-}$ enamel organ. (A–D) *In situ* hybridization analysis of ferritin heavy chain mRNA of wild-type (A, B) and *Nrf2*$^{-/-}$ (C, D) mouse enamel organs. (E–H) Immunohistochemical analysis of ferritin in the wild-type (E, F) and *Nrf2*$^{-/-}$ (G, H) mouse enamel organs. (A, C, E, G) show the transition stage, while (B, D, F, H) show the late maturation stage of ameloblast maturation. AM, ameloblasts; PA, Papillary cell layer.

ameloblasts underwent severe degenerative changes and disappeared prematurely during their maturation stages, so the loss of the ameloblast function resulted in the failure of iron deposition to the enamel surface and the decolourization of the incisors. To our knowledge, this is the first report describing the iron metabolism disorder in the *Nrf2*$^{-/-}$ mouse.

Iron is critically involved in various cellular events ranging from DNA synthesis to cellular respiration (Cammack *et al.* 1990). Among them, the iron utilization

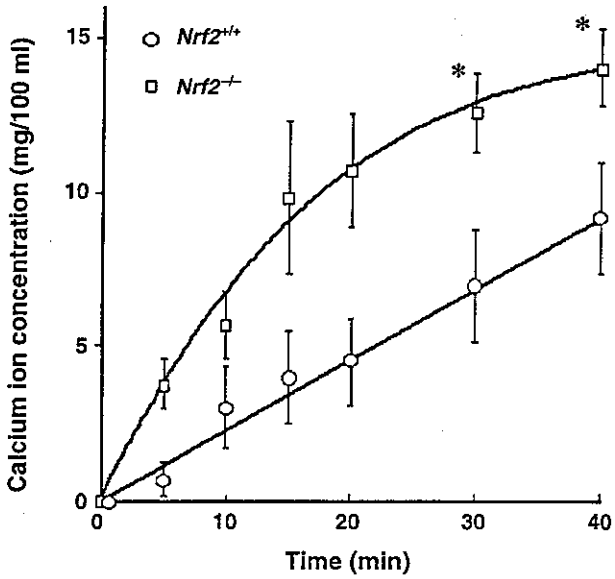

Figure 6 $Nrf2^{-/-}$ mice incisors have diminished acid resistance. A 0.5 mm × 5 mm area of the buccal surface of murine incisors was exposed to acetate buffer at pH 4.0, and the amount of eluted calcium ion was determined. The surface of the $Nrf2^{-/-}$ tooth (□) eroded significantly earlier in acetic acid than that of the wild-type mice (○). $*P < 0.05$: Student's t-test.

in the rodent enamel organ illustrates one of the most interesting examples of iron usage in mammals. Iron deposited on to the enamel surface seems to contribute to the formation of acid resistance and hardness of the rodent incisors, which is advantageous for grinding the hard seeds in the environment (Halse 1974; Stein & Boyle 1959). In fact, the diminished acid resistance of iron-poor $Nrf2^{-/-}$ teeth (Fig. 6) supports the notion that the iron deposition in the enamel surface is an important event to preserve the rodent tooth function.

In terms of the iron and calcium transport, as well as matrix and water removal, the papillary layer cells have been shown to form an intimate functional unit with the ameloblasts during early to late stages of the enamel maturation (Ohshima *et al.* 1998; Garant & Gillespie 1969; Skobe & Garant 1974). Importantly, transferrin receptors are found to be mainly expressed in the papillary layer cells of the enamel organ of rat incisors (Mataki *et al.* 1989), suggesting that the papillary layer cells uptake iron efficiently from the circulating blood. Although mechanism of the next transfer process of iron, i.e. from the papillary layer cells to ameloblasts, is not well understood at present, one plausible explanation for this is that the transferrin-bound iron from the circulating blood may be transferred to ferritin within the papillary layer cells, and subsequently the ferritin-bound iron is transferred to ameloblasts. Consistent with this contention, we observed high ferritin protein accumulation both in the ameloblasts and papillary layer cells in the wild-type enamel organ.

Ferritin serves as the transient iron reservoir in mature ameloblasts, and surprisingly the ameloblasts express ferritin mRNA most abundantly amongst rat tissues (Miyazaki *et al.* 1998). Ferritin is a 480-kDa intracellular protein that can store up to 4500 atoms of iron. The protein consists of heavy and light chains. The ratio of subunits within a ferritin molecule varies widely from tissue to tissue, which in turn modulates the ferritin function (Miyazaki *et al.* 1998). Although ferritin is expressed at equal levels both in ameloblasts and papillary layer cells in the wild-type enamel organ, the *in situ* analysis of ferritin heavy chain mRNA expression demonstrates that the mRNA is exclusively expressed in the ameloblasts. This observation suggests that the ferritin synthesized in the ameloblasts may be transferred to the papillary cells (Mataki *et al.* 1989). An alternative, and less likely, possibility is that the expression of ferritin mRNA in papillary cells might be under the detection limit of the *in situ* hybridization method and efficient translation compensated for the weak expression of the gene at mRNA level.

While ferritin is abundantly accumulated, iron accumulation is scarcely observed in the papillary layer cells of the wild-type mouse. This observation suggests that the iron transfer process from the papillary layer cells to ameloblasts may be very efficient in the wild-type enamel organ. We envisage that ferritin may be loaded with iron in the papillary layer cells and rapidly transferred to the ameloblasts.

An important observation is that the accumulation level of ferritin is abnormally reduced, but accumulation level of iron is abnormally increased, in the $Nrf2^{-/-}$ papillary layer cells, suggesting that the iron transfer process is somehow disturbed in the $Nrf2^{-/-}$ enamel organ. We envisage the following scenario to explain the observation, which is depicted schematically in Fig. 7. Since the expression levels of ferritin heavy chain mRNA and ferritin protein in the $Nrf2^{-/-}$ ameloblasts was almost comparable to those of the wild-type ameloblasts (see Fig. 5), a translocation or recycling step of ferritin from the ameloblasts to the papillary layer cells might be affected in the $Nrf2^{-/-}$ mice (Radisky & Kaplan 1998; Kwok & Richardson 2003). Although the translocation of ferritin from ameloblasts to papillary layer cells has not been evidenced to date, such a mechanism might be affected in $Nrf2^{-/-}$ enamel organ most probably because of the enhanced oxidative stress in ameloblasts.

An alternative explanation is that the decrease in the ferritin mRNA expression may be involved in the

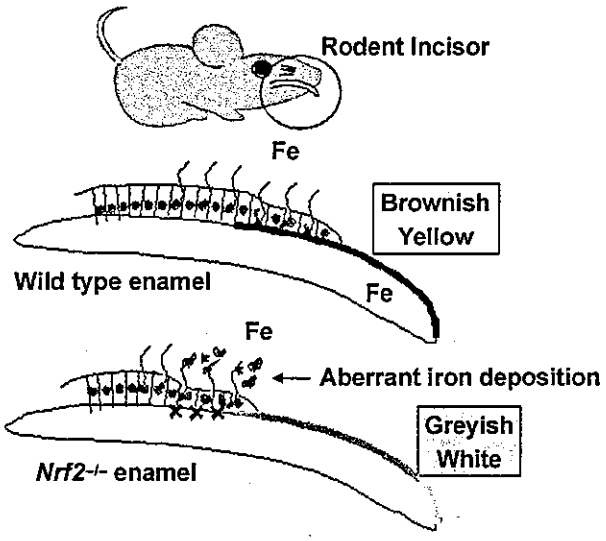

Figure 7 *Nrf2*$^{-/-}$ mice were defective in iron utilization in developing enamel organ. *Nrf2*$^{-/-}$ teeth were greyish white (bottom panel), whereas those of wild-type mice were brownish yellow (middle panel). This decolourization is owing to the defect of iron deposition in the mature enamel surface. *Nrf2*$^{-/-}$ enamel organs have iron transport defect that leads to both enamel cell degeneration and disturbed iron deposition on to the enamel surface. Brown arrows designate the direction of iron transport and subsequent deposition.

decrease of ferritin in the *Nrf2*$^{-/-}$ papillary cells. Indeed, it was recently reported that the chemical activators of Nrf2 up-regulates the ferritin heavy and light chain gene expression *in vivo*, indicating that the ferritin gene expression is under the regulation of Nrf2/ARE pathway (Primiano *et al.* 1996; Tsuji *et al.* 2000; Pietsch *et al.* 2003). Supporting this contention, it was also reported that the expression of ferritin genes is not induced, but basal level of the gene expression is rather reduced in *Nrf2*$^{-/-}$ mouse embryonic fibroblasts (Pietsch *et al.* 2003). Moreover, decrease in the basal expression as well as the induction of ferritin gene was found in *Nrf2*$^{-/-}$ astrocytes (Lee *et al.* 2003). The basal level expression of ferritin mRNA in *Nrf2*$^{-/-}$ small intestine was also decreased in a microarray analysis (Thimmulappa *et al.* 2002). Thus, further analyses is required to clarify the underlying mechanisms of iron transport defect observed in *Nrf2*$^{-/-}$ enamel organ.

The aberrant accumulation of iron in *Nrf2*$^{-/-}$ papillary cells seems to lead the ameloblasts to premature degeneration by oxidative stress, as iron generates highly reactive oxygen species via Fenton chemistry and causes an oxidative stress to cells (Linn 1998). Upon utilization of iron therefore cells need to be equipped with an array of anti-oxidant systems to prevent its toxicity. Since Nrf2 regulates expression of the genes that protect cells from oxidative stress (Ishii *et al.* 2000; Itoh *et al.* 1999b), there is a possibility that defective expression of certain Nrf2/ARE-regulated gene(s) might be involved in the degenerative changes observed in the *Nrf2*$^{-/-}$ enamel organ. For the understanding of the iron transport system that is defective in the *Nrf2*$^{-/-}$ mouse, comprehensive as well as quantitative analyses of the expression of ARE-regulated genes in the enamel organ is critically important. However, we need a technical breakthrough for collecting enough amounts of mouse enamel organs for such analyses.

Experimental procedures

Macroscopic observation

The generation of *Nrf2* gene mutant mice was previously described (Itoh *et al.* 1997). The incidence of decolourization phenotype was analysed by the χ^2-test.

Scanning electron microscopic observation and micro X-ray analysis

The murine incisors, including maxillary bones, were fixed in 100% ethanol and dehydrated by the critical point drying method. The incisors from *Nrf2*$^{+/-}$ and *Nrf2*$^{-/-}$ mice were examined using a scanning electron microscope (Hitachi S-2500CX) operated at 15 kV. Micro X-ray analysis was performed to determine the chemical components of the incisors. For energy-dispersive X-ray analysis, an X-ray detector system (Kevex Quantum Delta IV) attached to a scanning electron microscope was used. The micro X-ray analysis system was operated at a 15-kV accelerating voltage and a 0.1-nA probe current, with a 20-nm probe size and a 100-s counting time. Five points on the enamel surface were selected and analysed for the amounts of calcium, phosphorus and iron. The iron concentration was detected in 1 μm depth of enamel surface.

In situ hybridization, immunohistochemistry and iron staining

Ferritin heavy chain cDNA was subcloned into the pBluescript KS$^+$ vector and used as a template for cRNA production. DIG-11-UTP-labelled single-strand anti-sense and sense RNA probes were prepared by DIG-RNA Labeling Kit (Behringer Mannheim) according to the manufacturer's instruction. Samples were fixed with 4% paraformaldehyde with PBS overnight at 4 °C and decalcified in 10% EDTA (pH 7.4) for 2 weeks, embedded in paraffin and sectioned. *In situ* hybridization was performed as previously described (Shibata *et al.* 2000). After treatment with 0.2 N hydrochloric acid and Proteinase K (10 μg/mL), hybridization was performed with the probe (1 μg/mL) at 50 °C overnight. After extensive washing and RNase A treatment, the hybridized DIG-labelled probes were detected with alkaline phosphatase-

conjugated anti-DIG antibody and 5-bromo-4-chloro-3-indolyl phosphate as the substrate, using a nucleic acid detection kit (Behringer Manheim).

Immunostaining was performed using the labelled streptavidin biotin method (LsAB method: Nichirei). Sections were immersed in 0.3% hydrogen peroxide in methanol for 30 min, and incubated with 5% normal goat serum for 30 min at room temperature. The sections were then incubated with anti-rat liver ferritin rabbit polyclonal antibody (1 : 200 v/v) in PBS at 4 °C overnight (Miyazaki *et al.* 1998). The slides were reacted with biotinylated goat anti-rabbit antibody for 30 min at room temperature, followed by horseradish peroxidase conjugated with streptavidin. The peroxidase activity was visualized by the 3-amino-9-ethylcarbasol substrate-chromogen system (Nichirei, Tokyo). The sections were counterstained with haematoxylin, dehydrated, and mounted. Control staining was performed with non-immune rabbit serum. Berlin blue staining was performed to detect iron deposits.

Serum iron parameters and liver iron content

Blood was obtained from abdominal aorta of anaesthetized mice and 200 μL of serum from each animal was used for analysis of iron and total iron binding capacity. These assays were performed by SRL Inc. (Tokyo) using an automatic chemical analyser (Hitachi). Non-haem iron in the liver was measured as previously described (Foy *et al.* 1967).

Analysis of acid resistance and Knoop hardness

Hardness test of the enamel surface was performed by using a hardness tester equipped with a Knoop penetrator. Six kg load was applied to each tooth for 10 s. To measure the acid resistance of the teeth, a 5 mm × 0.5 mm of the buccal surface of the murine incisors was exposed to 100 μL of acetate buffer (100 mM) at pH 4.0 at room temperature. The eluted calcium ion was measured by the methylxylenol blue method (Calcium *E*-test Wako, Wako, USA) at 5, 10, 15, 20, 30 and 40 min. The means from five independent incisors from 8 to 12-week-old mice were presented with standard errors.

Acknowledgements

We thank Dr Takanobu Isokawa and *Kitl*. Tong for discussion and advice. This work was supported in part by grants from JST-ERATO, JSPS, the Ministry of Education, Culture, Sports, Science and Technology, the Ministry of Health, Labor and Welfare, CREST, and the Naito foundation.

References

Aoki, Y., Sato, H., Nishimura, N., Takahashi, S., Itoh, K. & Yamamoto, M. (2001) Accelerated DNA adduct formation in the lung of the Nrf2 knockout mouse exposed to diesel exhaust. *Toxicol. Appl. Pharmacol.* **173**, 154–160.

Cammack, R., Wriggleworth, J.M. & Baum, H. (1990) Iron dependent enzymes in mammalian systems. In: *Iron Transport and Storage* (eds P. Ponka, H. M. Schulman & R. C. Woodworth), pp. 17–40. Boca Raton: CRC Press.

Chan, K., Han, X.D. & Kan, Y.W. (2001) An important function of Nrf2 in combating oxidative stress: detoxification of acetaminophen. *Proc. Natl. Acad. Sci. USA* **98**, 4611–4616.

Chan, K. & Kan, Y.W. (1999) Nrf2 is essential for protection against acute pulmonary injury in mice. *Proc. Natl. Acad. Sci. USA* **96**, 12731–12736.

Cho, H.Y., Jedlicka, A.E., Reddy, S.P., *et al.* (2002) Role of NRF2 in Protection Against Hyperoxic Lung Injury in Mice. *Am. J. Respir. Cell. Mol. Biol.* **26**, 175–182.

Enomoto, A., Itoh, K., Nagayoshi, E., *et al.* (2001) High sensitivity of Nrf2 knockout mice to acetaminophen hepatotoxicity associated with decreased expression of ARE-regulated drug metabolizing enzymes and antioxidant genes. *Toxicol. Sci.* **59**, 169–177.

Foy, A.L., Williams, H.L., Cortell, S. & Conrad, M.E. (1967) A modified procedure for the determination of non-heme iron in tissue. *Anal. Biochem.* **18**, 559–563.

Garant, P.R. & Gillespie, R. (1969) The presence of fenestrated capillaries in the papillary layer of the enamel organ. *Anat. Rec.* **163**, 71–79.

Halse, A. (1973) Effect of dietary iron deficiency on the pigmentation and iron content of rat incisor enamel. *Scand. J. Dent. Res.* **81**, 319–334.

Halse, A. (1974) Electron microprobe analysis of iron content of incisor enamel in some species of Rodentia. *Arch. Oral. Biol.* **19**, 7–11.

Halse, A. & Selvig, K.A. (1974) Incorporation of iron in rat incisor enamel. *Scand. J. Dent. Res.* **82**, 47–56.

Ishii, T., Itoh, K., Takahashi, S., *et al.* (2000) Transcription factor Nrf2 coordinately regulates a group of oxidative stress-inducible genes in macrophages. *J. Biol. Chem.* **275**, 16023–16029.

Itoh, K., Chiba, T., Takahashi, S., *et al.* (1997) An Nrf2/small maf heterodimer mediates the induction of phase II detoxifying enzyme genes through antioxidant responsive element. *Biochem. Biophys. Res. Commun.* **236**, 313–322.

Itoh, K., Igarashi, K., Hayashi, N., Nishizawa, M. & Yamamoto, M. (1995) Cloning and characterization of a novel erythroid cell-derived CNC family transcription factor heterodimerizing with the small maf family proteins. *Mol. Cell. Biol.* **15**, 4184–4193.

Itoh, K., Ishii, T., Wakabayashi, N. & Yamamoto, M. (1999a) Regulatory mechanisms of cellular response to oxidative stress. *Free Radic. Res.* **31**, 319–324.

Itoh, K., Wakabayashi, N., Katoh, Y., *et al.* (1999b) Keap1 represses nuclear activation of antioxidant responsive elements by Nrf2 through binding to the amino-terminal Neh2 domain. *Genes Dev.* **13**, 76–86.

Kallenbach, E. (1970) Fine structure of rat incisor enamel organ during late pigmentation and regression stages. *J. Ultrastruct. Res.* **30**, 38–63.

Karim, A. & Warshawsky, H. (1984) A radioautographic study of the incorporation of iron 55 by the ameloblasts in the zone of maturation of rat incisors. *Am. J. Anat.* **169**, 327–335.

Kuroha, T., Takahashi, S., Komeno, T., Itoh, K., Nagasawa, T. & Yamamoto, M. (1998) Ablation of Nrf2 function does not

increase the erythroid or megakaryocytic cell lineage dysfunction caused by p45 NF-E2 gene disruption. *J. Biochem.* **123**, 376–379.

Kwok, J.C. & Richardson, D.R. (2003) Anthracyclines induce accumulation of iron in ferritin in myocardial and neoplastic cells: inhibition of the ferritin iron mobilization pathway. *Mol. Pharmacol.* **63**, 849–861.

Lee, J.M., Calkins, M.J., Chan, K., Kan, Y.W. & Johnson, J.A. (2003) Identification of the NF-E2-related factor-2-dependent genes conferring protection against oxidative stress in primary cortical astrocytes using oligonucleotide microarray analysis. *J. Biol. Chem.* **278**, 12029–12038.

Linn, S. (1998) DNA damage by iron and hydrogen peroxide in vitro and in vivo. *Drug Metab. Rev.* **30**, 313–326.

Mataki, S., Ohya, M., Kubota, M., Ino, M. & Ogura, H. (1989) Immunohistochemical and pharmacological studies on the distribution of ferritin and its secretory process of amelolasts in rat incisor enamel. In: *Tooth Enamel* (ed. R. W. Fearnhead), pp. 108–112. Yokohama: Yokohama Florence Publishers.

McCord, J.M. (1998) Iron, free radicals, and oxidative injury. *Semin. Hematol.* **35**, 5–12.

Miyazaki, Y., Sakai, H., Shibata, Y., Shibata, M., Mataki, S. & Kato, Y. (1998) Expression and localization of ferritin mRNA in ameloblasts of rat incisor. *Arch. Oral. Biol.* **43**, 367–378.

Mohler, J., Vani, K., Leung, S. & Epstein, A. (1991) Segmentally restricted, cephalic expression of a leucine zipper gene during Drosophila embryogenesis. *Mech. Dev.* **34**, 3–9.

Ohshima, H., Maeda, T. & Takano, Y. (1998) Cytochrome oxidase activity in the enamel organ during amelogenesis in rat incisors. *Anat. Rec.* **252**, 519–531.

Pietsch, E.C., Chan, J.Y., Torti, F.M. & Torti, S.V. (2003) Nrf2 mediates the induction of ferritin H in response to xenobiotics and cancer chemopreventive dithiolethiones. *J. Biol. Chem.* **278**, 2361–2369.

Primiano, T., Kensler, T.W., Kuppusamy, P., Zweier, J.L. & Sutter, T.R. (1996) Induction of hepatic heme oxygenase-1 and ferritin in rats by cancer chemopreventive dithiolethiones. *Carcinogenesis.* **17**, 2291–2296.

Radisky, D.C. & Kaplan, J. (1998) Iron in cytosolic ferritin can be recycled through lysosomal degradation in human fibroblasts. *Biochem. J.* **336**, 201–215.

Ramos-Gomez, M., Kwak, M.K., Dolan, P.M., *et al.* (2001) Sensitivity to carcinogenesis is increased and chemoprotective efficacy of enzyme inducers is lost in nrf2 transcription factor-deficient mice. *Proc. Natl. Acad. Sci. USA* **98**, 3410–3415.

Shibata, Y., Fujita, S., Takahashi, H., Yamaguchi, A. & Koji, T. (2000) Assessment of decalcifying protocols for detection of specific RNA by non-radioactive in situ hybridization in calcified tissues. *Histochem. Cell Biol.* **113**, 153–159.

Skobe, Z. & Garant, P.R. (1974) Electron microscopy of horseradish peroxidase uptake by papillary cells of the mouse incisor enamel organ. *Arch. Oral. Biol.* **19**, 387–395.

Stein, G. & Boyle, P.E. (1959) Pigmentation of the enamel of albino rat incisor teeth. *Arch. Oral Biol.* **1**, 97–105.

Takano, Y. & Ozawa, H. (1981) Cytochemical studies on the ferritin-containing vesicles of the rat incisor ameloblasts with special reference to the acid phosphatase activity. *Calcif. Tissue Int.* **33**, 51–55.

Thimmulappa, R.K., Mai, K.H., Srisuma, S., Kensler, T.W., Yamamoto, M. & Biswal, S. (2002) Identification of Nrf2-regulated genes induced by the chemopreventive agent sulforaphane by oligonucleotide microarray. *Cancer Res.* **62**, 5196–5203.

Tsuji, Y., Ayaki, H., Whitman, S.P., Morrow, C.S., Torti, S.V. & Torti, F.M. (2000) Coordinate transcriptional and translational regulation of ferritin in response to oxidative stress. *Mol. Cell. Biol.* **20**, 5818–5827.

Yoh, K., Itoh, K., Enomoto, A., *et al.* (2001) Nrf2 deficient female mice develop lupus-like autoimmune nephritis. *Kidney Int.* **60**, 1343–1353.

Received: 10 January 2004
Accepted: 13 April 2004

THE JOURNAL OF BIOLOGICAL CHEMISTRY
© 2004 by The American Society for Biochemistry and Molecular Biology, Inc.

Vol. 279, No. 30, Issue of July 23, pp. 31556–31567, 2004
Printed in U.S.A.

Redox-regulated Turnover of Nrf2 Is Determined by at Least Two Separate Protein Domains, the Redox-sensitive Neh2 Degron and the Redox-insensitive Neh6 Degron*[S]

Received for publication, March 19, 2004, and in revised form, May 12, 2004
Published, JBC Papers in Press, May 13, 2004, DOI 10.1074/jbc.M403061200

Michael McMahon‡§, Nerys Thomas‡, Ken Itoh¶, Masayuki Yamamoto¶, and John D. Hayes‡

From the ‡Biomedical Research Centre, Ninewells Hospital and Medical School, University of Dundee, Dundee DD1 9SY, Scotland, United Kingdom and ¶Centre for Tsukuba Advanced Research Alliance and Institute of Basic Medical Sciences, University of Tsukuba, Tsukuba 305-8577, Japan

The Nrf2 transcription factor is more rapidly turned over in cells grown under homeostatic conditions than in those experiencing oxidative stress. The variable turnover of Nrf2 is accomplished through the use of at least two degrons and its redox-sensitive interaction with the Kelch-repeat protein Keap1. In homeostatic COS1 cells, the Neh2 degron confers on Nrf2 a half-life of less than 10 min. Analyses of deletion mutants of a Gal4(HA)mNeh2 fusion protein and full-length mNrf2 indicate that full redox-sensitive Neh2 destabilizing activity depends upon two separate sequences within this N-terminal domain. The DIDLID element (amino acids 17–32) is indispensable for Neh2 activity and appears necessary to recruit a ubiquitin ligase to the fusion protein. A second motif within Neh2, the ETGE tetrapeptide (amino acids 79–82), allows the redox-sensitive recruitment of Nrf2 to Keap1. This interaction, which occurs only in homeostatic cells, enhances the capacity of the Neh2 degron to direct degradation by functioning downstream of ubiquitination mediated by the DIDLID element. By contrast with the situation under homeostatic conditions, the Neh2 degron is neither necessary nor sufficient to account for the characteristic half-life of Nrf2 in oxidatively stressed cells. Instead, the previously uncharacterized, redox-insensitive Neh6 degron (amino acids 329–379) is essential to ensure that the transcription factor is still appropriately turned over in stressed cells, albeit with an increased half-life of 40 min. A model can now be proposed to explain how the turnover of this protein adapts in response to alterations in cellular redox state.

The Nrf2 transcription factor regulates many antioxidant and detoxification genes in response to oxidative insult (1–3). The resulting biochemical alterations enhance the capacity of cells to survive the stress by detoxifying the causative agent along with by-products of the stress, by repairing or recycling damaged macromolecules, and ultimately, restoring redox homeostasis. The pivotal role of Nrf2 in this adaptive response is clear from the lack of up-regulation of these genes in mice lacking this factor (4–7).

Induction of many genes in response to oxidative stress occurs through the antioxidant-response element (ARE)[1] (for a review, see Ref. 8). This enhancer is bound by "cnc" bZIP proteins, which consists of not only Nrf2 but also the p45 subunit of NF-E2, Nrf1, and Nrf3, and the more distantly related members Bach1 and Bach2. These proteins bind AREs as obligate heterodimers with any one of three small Maf proteins (MafF, MafG, and MafK), which may themselves also bind as homodimers (for a review, see Ref. 9). Furthermore, other bZIP proteins are reputed to bind this enhancer (9). The transcriptional state of ARE-regulated genes is determined by the identity of the dimer recruited. For example, small Maf homodimers, which lack transactivation domains, are not competent to drive transcription from this element (Ref. 10), and Bach1-containing heterodimers actively repress transcription (11). In comparison, Nrf2 has been shown to be a strong transactivator, and its recruitment to an ARE, as a heterodimer with a small Maf partner molecule, results in transcriptional up-regulation of the gene in question (1, 12). The existence of functionally distinct bZIP dimers allows the cell to control ARE-driven gene transcription by varying the quantity of specific cnc and small Maf proteins in the nucleus and, therefore, the spectrum of dimers expressed. Accordingly, cellular adaptation to oxidative stress involves, among other changes, a rapid increase in the nuclear level of Nrf2 (13–15), possibly coupled with a decrease in the amount of Bach1 (16), leading in turn to enhanced recruitment of Nrf2-containing dimers to the promoters of ARE-regulated genes (17).

The amount of Nrf2 protein in the nucleus is controlled by the cytoplasmic, actin-bound protein, Keap1 (Kelch-like ECH-associated protein 1). ECH (erythroid cell-derived protein with cnc homology) is a synonym for *Gallus gallus* Nrf2. This Kelch-repeat protein was originally identified because it can interact with the N-terminal Neh2 (Nrf2-ECH homology 2) domain of Nrf2. Subsequently, Keap1 was found to bind directly to Nrf2 via an ETGE tetrapeptide motif within Neh2 (18–19). Initial overexpression assays indicated that Keap1 dictates the subcellular localization of Nrf2. It was demonstrated to tether Nrf2 in the cytoplasm of homeostatic cells, but during oxidative stress this interaction was antagonized, leaving Nrf2 free to translocate to the nucleus (18).

* This work was supported by the Association for International Cancer Research Grant 03-074 and the World Cancer Research Fund Grant 2002/55. The costs of publication of this article were defrayed in part by the payment of page charges. This article must therefore be hereby marked "*advertisement*" in accordance with 18 U.S.C. Section 1734 solely to indicate this fact.

[S] The on-line version of this article (available at http://www.jbc.org) contains Supplemental Figs. 1–4.

§ To whom correspondence should be addressed: Biomedical Research Centre, Ninewells Hospital and Medical School, Dundee DD1 9SY, Scotland, UK. Tel.: 0044-1382-660111; Fax: 0044-1382-669993; E-mail: m.j.m.mcmahon@dundee.ac.uk.

[1] The abbreviations used are: ARE, antioxidant response element; BTB, Broad-complex, Tramtrack, and Bric-a-brac; CHX, cycloheximide; cnc, cap 'n collar; ER, endoplasmic reticulum; HA, hemagglutinin; Keap1, Kelch-like ECH-associated protein 1; Neh, Nrf2-ECH homology; Nrf, NF-E2-related factor; Sul, sulforaphane; Ubl, ubiquitin-like; E1, ubiquitin-activating enzyme.

Recent studies (13–15, 20–21) indicate that oxidative stress influences not only the subcellular distribution of Nrf2 but also the total amount of Nrf2. Thus, in the nontransformed RL34 rat liver epithelial cell line, rNrf2 protein was undetectable under homeostatic conditions, but levels of the protein increased rapidly in the nucleus following treatment with sulforaphane (Sul), a model oxidative stressor (15). To account for these findings, it has been proposed that Keap1 both sequesters Nrf2 in the cytoplasm and enhances proteasomal degradation of the transcription factor in homeostatic cells (14, 15). Consistent with this model, we have demonstrated previously in COS1 cells that both the steady-state level of Nrf2 protein and its half-life are redox-sensitive, when coexpressed with Keap1. Deletion of the ETGE tetrapeptide motif from the Neh2 domain of Nrf2 demonstrated that its redox-sensitive interaction with Keap1 underpins its decreased stability during homeostatic conditions (15). To our surprise, although interaction with Keap1 enhanced the rate of proteasomal degradation of Nrf2 in homeostatic cells, the interaction did not enhance ubiquitination of the bZIP factor (15). Further examination of how the Neh2 domain controls protein half-life revealed that it does not simply contain the interaction site for Nrf2 and Keap1 but that this region is a redox-sensitive degron. Specifically, when Neh2 was fused to Gal4 and coexpressed with Keap1, the half-life of the recombinant protein was reduced, and its steady-state level became redox-sensitive. Deletion of the ETGE motif from the fusion protein also showed that the Neh2 domain could mediate proteasomal degradation independently of its interaction with Keap1. We thus proposed that Nrf2 is capable of being degraded proteasomally, via its Neh2 degron, both dependently and independently of Keap1. Under homeostatic conditions, the Neh2 degron mediates a rapid, Keap1-dependent degradation of Nrf2 (15). By contrast, under conditions of oxidative stress, the Neh2 degron directs a less rapid, Keap1-independent degradation of the bZIP factor.

The relationship between Keap1-dependent and -independent Neh2-mediated degradation is unclear. It is not known whether Keap1 simply acts to enhance the rate of the Keap1-independent mechanism or whether several pathways for Nrf2 degradation exist.

Comparison of the amino acid sequence of SKN-1, a transcription factor in *Caenorhabditis elegans* that responds to oxidative stress, with that of Nrf2 has revealed the presence of a conserved peptide called the "DIDLID element" in the nematode protein (22). This element is located between residues 99 and 112 of SKN-1, whereas in mouse, rat, and human Nrf2 it resides in the Neh2 domain between amino acids 17 and 32 (Fig. 1). In SKN-1, the DIDLID element is part of a transactivation domain, although this property is also shared with other regions of the nematode factor. The function of the region in Nrf2 homologous to the SKN-1 DIDLID element is not known, but the striking conservation suggests it performs an essential role. Given the fact that Neh2 helps control the turn over of Nrf2, it is important to establish whether the Neh2 subdomain equivalent to the SKN-1 element contributes to this process. Besides Neh2, five additional domains, Neh1, Neh3, Neh4, Neh5, and Neh6, have been identified in Nrf2. It is not known if these regions contribute to the destabilization of the bZIP protein.

In this paper we report for the first time that ubiquitination of a Gal4(HA)mNeh2 fusion protein depends upon the subdomain equivalent to the DIDLID element in SKN-1. By deleting amino acids 17–32 from full-length mNrf2, we demonstrate that Keap1 functions to enhance the rate of degradation of Nrf2 by acting downstream of ubiquitination directed by the DIDLID element. Whereas the Neh2 domain is both necessary and sufficient for degradation of Nrf2 in homeostatic cells, it can be removed without altering the turnover rate of the protein in oxidatively stressed cells. Instead, degradation of the protein in stressed cells is predominantly mediated by the previously unrecognized, redox-insensitive Neh6 degron.

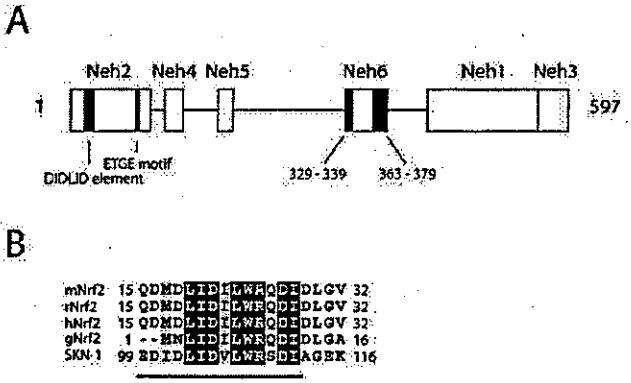

FIG. 1. **Structure of Nrf2.** *A*, schematic of the conserved domain structure of mouse Nrf2 based on a sequence alignment of orthologous Nrf2 proteins is presented. Conserved domains are referred to as Neh domains. The DIDLID element (amino acids 17–32) and the ETGE motif (amino acids 79–82) of the Neh2 domain are highlighted, as are two highly conserved regions of the Neh6 domain (amino acids 329–339 and 363–379). A complete sequence alignment of orthologous Nrf2 proteins from human to fish and a description of the known functions of the Neh domains can be found in the supplemental Fig. 1. *B*, a comparison of the regions of mouse (*m*), rat (*r*), human (*h*), and chicken (*g*) Nrf2 proteins encompassing DIDLID elements, and the corresponding sequence from *C. elegans* SKN-1 protein is presented. The sequence defined as the DIDLID element in SKN-1 is *underlined*. In the context of mNrf2, we use the term to refer to amino acids 17–32.

EXPERIMENTAL PROCEDURES

Plasmids—pCG-GAL(HA), which expresses a hemagglutinin (HA)-tagged GAL4 DNA-binding domain was a kind gift of Dr. William P. Tansey (Cold Spring Harbor Laboratory, NY) and has been described in Ref. 23. pCG-GAL(HA)mNeh6, which expresses Gal4(HA)mNeh6, a HA-tagged Gal4 DNA-binding domain fused to the Neh6 domain of mNrf2, was generated by PCR amplification of the region coding amino acids 318–401 by using the primer pair 5′-GACCTGTCACTGTCTAGAGCTTTCAACCCG-3′ and 5′-CATAGGAGCACTGGATCCTTGCTATGGTGACAGAGGCTG-3′. The resulting product was digested with XbaI and BamHI and ligated into similarly digested pCG-GAL(HA). pCG-GAL(HA)mNeh2, which expresses Gal4(HA)mNeh2, a hemagglutinin (HA)-tagged GAL4 DNA-binding domain-mNeh2 fusion protein, has been described previously, as has pcDNA3.1/V5mNrf2, which expresses full-length mNrf2 tagged at the C terminus with a V5 epitope (mNrf2-V5) (15). All constructs expressing the deletion mutants of Gal4(HA)mNeh2 or mNrf2-V6 mentioned in the text were generated from the above parental vectors by deletion mutagenesis using the GeneEditor kit (Promega). The sequences of the mutagenic oligonucleotides used are available on request. pcDNA3.1/V5HisCmKeap1 and pcDNA3.1/mKeap1, which express mKeap1-V5-hexahistidine and untagged mKeap1, respectively, have been described previously (15). The pARE-164CAT reporter construct was a gift from Dr. Cecil B. Pickett (Schering Plough Research Institute, Kenilworth, NJ) and has been described previously (24). pCMVβ-gal (Clontech) expresses β-galactosidase under the control of a cytomegalovirus promoter and was included in all transfections as an internal control. pHisUb, which expresses hexahistidine-tagged octameric ubiquitin precursor protein from a cytomegalovirus promoter (25), was provided by Prof. David P. Lane (University of Dundee). All constructs prepared for this study were sequence-verified.

Cell Culture, Transfections, Chemical Challenge, and Reporter Assays—ts20TG^R and H38.5 cells (26) were kind gifts from Profs. Harvey L. Ozer (University of Medicine and Dentistry of New Jersey-New Jersey Medical School) and Christoph Borner (Albert-Ludwigs University, Freiburg, Germany). The ts20TG^R cell line harbors a temperature-sensitive mutant E1 enzyme. The mutant enzyme permits growth at 34.5 °C but is inactivated by shifting cells to the nonpermissive temperature of 39 °C. This cell line was maintained at 34.5 °C in Dulbecco's

modified Eagle's medium (Invitrogen) supplemented with 10% (v/v) heat-inactivated fetal calf serum (Invitrogen) and penicillin-streptomycin. The H38.5 cell line was derived from the ts20TG^R cell line and contains stably integrated DNA expressing the wild-type E1 protein. It was maintained as for the parent cell line, but its growth medium was supplemented with 50 μg/ml hygromycin B (Sigma) to maintain the integrated DNA. COS1 cells were grown in Dulbecco's modified Eagle's medium (Invitrogen) supplemented with 10% (v/v) heat-inactivated fetal calf serum (Invitrogen) and penicillin-streptomycin. RL34, non-transformed rat liver epithelial cells, were maintained in Dulbecco's modified Eagle's medium (Invitrogen) supplemented with 10% (v/v) heat-inactivated fetal calf serum (Invitrogen), 2 mM L-glutamine, and penicillin-streptomycin. Cells were seeded into either 6-well plates or 60-mm tissue culture dishes at least 18 h before transfection and were ~50% (ts20TG^R, H38.5, or RL34 cells) or 90% (COS1 cells) confluent at the time of transfection. Cells were transfected using either Lipofectin (COS1) or LipofectAMINE 2000 (ts20TG^R, H38.5, or RL34 cells) (both products from Invitrogen) according to the manufacturer's instructions. Cells were challenged with chemicals not less than 40 h after plating. Sul was obtained from LKT Laboratories. Cycloheximide (CHX) was from Sigma. MG132 was from Calbiochem. The β-galactosidase and chloramphenicol acetyltransferase reporter assays were carried out as described previously (15).

Whole-cell Extracts, In Vivo Ubiquitination Assay, Immunoprecipitation, and Immunoblots—For immunoblots, whole-cell lysates were prepared by scraping cell monolayers into ice-cold radioimmune precipitation assay buffer (50 mM Tris-Cl, pH 7.4, 150 mM NaCl, 1% (v/v) Nonidet P-40, 0.5% (w/v) deoxycholic acid, 0.1% (w/v) SDS supplemented with complete, EDTA-free protease inhibitor mixture (Roche Applied Science)). Lysates were clarified by centrifugation (16,000 × *g*, 15 min, 4 °C). The *in vivo* ubiquitination assay was carried out, and subsequently, whole-cell lysates and His-tagged proteins fractions were prepared as described previously (15) with the following modification: cells were not pretreated with MG132 before preparing whole-cell and His-tagged samples. Immunoprecipitation of HA-tagged proteins from clarified, whole-cell lysates was by conventional methods. Briefly, 50 μl of mouse IgG-agarose (Sigma) was washed with radioimmune precipitation assay buffer by repeated centrifugation (5,000 × *g*, 2 min, 4 °C), and the resin was mixed with and used to preclear the lysate, by end-over-end tumbling at 4 °C for 1 h. The suspension was centrifuged (5,000 × *g*, 2 min, 4 °C), and the precleared lysate was added to 50 μl of mouse anti-HA (clone HA-7)-agarose (Sigma) and washed as described above. This was incubated overnight at 4 °C with continuous end-over-end mixing. The following morning, the resin was washed with 3 volumes of radioimmune precipitation assay buffer by repeated centrifugation (5,000 × *g*, 2 min, 4 °C). Material that remained bound to the resin was eluted in 50 μl of Laemmli reducing sample buffer. Protein determination, SDS-PAGE, and immunoblotting were carried out as described previously (15). Antibodies used included a rabbit anti-mNrf2 serum (15), 1:10,000, mouse anti-V5 (Invitrogen), 1:2000, mouse anti-HA (clone 12CA5-Roche Applied Science), 0.4 μg/ml, rabbit anti-Gal4 serum (Upstate Biotechnology, Inc.), 1:2000, and a Goat anti-hKeap1 antibody preparation (Santa Cruz Biotechnology), 0.8 μg/ml.

RESULTS

The DIDLID Element in Nrf2 Is Essential for Keap1-independent, Neh2-mediated Degradation—In an attempt to define more clearly the relationship between Keap1-independent and -dependent Neh2-directed degradation, a region within the N-terminal domain of Nrf2 was sought that is required for its turnover in a Keap1-independent fashion. Within the first 96 amino acids, which define the Neh2 degron, two regions are highly conserved: amino acids 1–55 and 65–85 (see supplemental Fig. 1). On the basis of this information, we generated expression constructs for Gal4(HA)mNeh2$^{\Delta 1-16}$, Gal4(HA)mNeh2$^{\Delta 17-32}$, Gal4(HA)mNeh2$^{\Delta 33-55}$, and Gal4(HA)mNeh2$^{\Delta 65-85}$ to determine which of the four subdomains within Neh2 might be responsible for Keap1-independent turn over of Nrf2.

The steady-state expression levels of these proteins were initially compared with that of Gal4(HA)mNeh2. Untagged Keap1 was coexpressed with all proteins, but the degradation observed was Keap1-independent as the level of expression of the fusion proteins was sufficiently great to saturate the capacity of heterologously expressed mKeap1 to affect degradation (Fig. 8 in Ref. 15, see below also). Steady-state levels were measured using antibodies against the Gal4 DNA-binding domain, the HA tag, and mNrf2. All three reagents gave similar results (Fig. 2*A*).[2] The amount of both the Gal4(HA)mNeh2$^{\Delta 1-16}$ and Gal4(HA)mNeh2$^{\Delta 17-32}$ proteins was higher in COS1 cells than the other three fusion proteins, all of which accumulated to similar extents (Fig. 2*A*). The half-life of each protein in COS1 cells was determined by CHX chase assay (Fig. 2*B*). Gal4(HA)mNeh2, Gal4(HA)mNeh2$^{\Delta 33-55}$, and Gal4(HA)mNeh2$^{\Delta 65-85}$ all had statistically indistinguishable half-lives of ~1 h. The fact that deleting amino acids 65–85 (and thus the ETGE motif required for Keap1 binding) did not affect the half-life of the fusion protein demonstrated that the observed degradation is accomplished by a Keap1-independent mechanism. In stark contrast, deletion of amino acids 17–32 resulted in a protein of greatly enhanced stability. This protein had a half-life of ~8 h in COS1 cells, and it was effectively metabolically stable. This presumably accounts for the fact that it was observed to accumulate to a much higher steady-state level than the Gal4-wild-type Neh2 fusion protein from which it was derived. Finally, whereas deletion of amino acids 1–16 enhance the stability of the fusion protein, its half-life only extends from 1 to 2 h, which on its own cannot fully account for the large increase in its protein level when compared with that of the intact Neh2 fusion protein. This discrepancy has been observed consistently, and we speculate that it reflects some alteration in the rate at which conformationally mature Gal4(HA)mNeh2$^{\Delta 1-16}$ is generated. The stabilization achieved by deleting amino acids 1–16 is far more modest than that accomplished by deletion of amino acids 17–32. It appears likely that the modest increase in the half-life of Gal4(HA)mNeh2$^{\Delta 1-16}$ occurs because the ability of amino acids 17–32 to direct degradation of the fusion protein is impaired by deletion of amino acids 1–16.

The DIDLID Element Directs Polyubiquitination of Gal4(HA)mNeh2—Targeting of substrates to the 26 S proteasome generally requires prior polyubiquitination, although exceptions to this rule exist (27–29). Thus, one interpretation of the above results is that the DIDLID element is essential for polyubiquitination of the fusion protein, possibly by recruiting an ubiquitin ligase. Thus, we sought to compare, under steady-state conditions, the fractions of Gal4(HA)mNeh2$^{\Delta 17-32}$ and wild-type proteins that are conjugated to ubiquitin, utilizing the His-tagged ubiquitination assay of Treier *et al.* (25). COS1 cells were transfected with the plasmids indicated in Fig. 3*A*, and 24 h later, both the total amount of fusion protein in a whole-cell lysate and the amount of fusion protein recovered in the affinity-purified His-tagged fraction were determined by immunoblot analysis. Fusion protein recovered in the His-tagged fraction represents the polyubiquitinated form of the protein as no such protein was recovered in this fraction unless both fusion protein and His-tagged ubiquitin were coexpressed (Fig. 3*A*, *lanes 7–10*).

Although the absolute amount of ubiquitinated Gal4(HA)mNeh2$^{\Delta 17-32}$ recovered at steady-state was effectively identical to that of the wild-type Neh2-fusion protein, a greater amount of the DIDLID deletion mutant had to be expressed to "drive" ubiquitination to this extent (Fig. 3*A*, *cf. lanes 1* and *2* with *lanes 5* and *6*). By making serial dilutions of the whole-cell fraction, it was estimated that the DIDLID deletion mutant accumulated to approximately eight times the

[2] The inability of the rabbit anti-mNrf2 antiserum to effectively react with Gal4(HA)mNeh2$^{\Delta 65-85}$ appears to be due to the fact that the deleted region is immunodominant and not due to misfolding of the Neh2 region in its absence (M. McMahon and J. D. Hayes, unpublished observations).

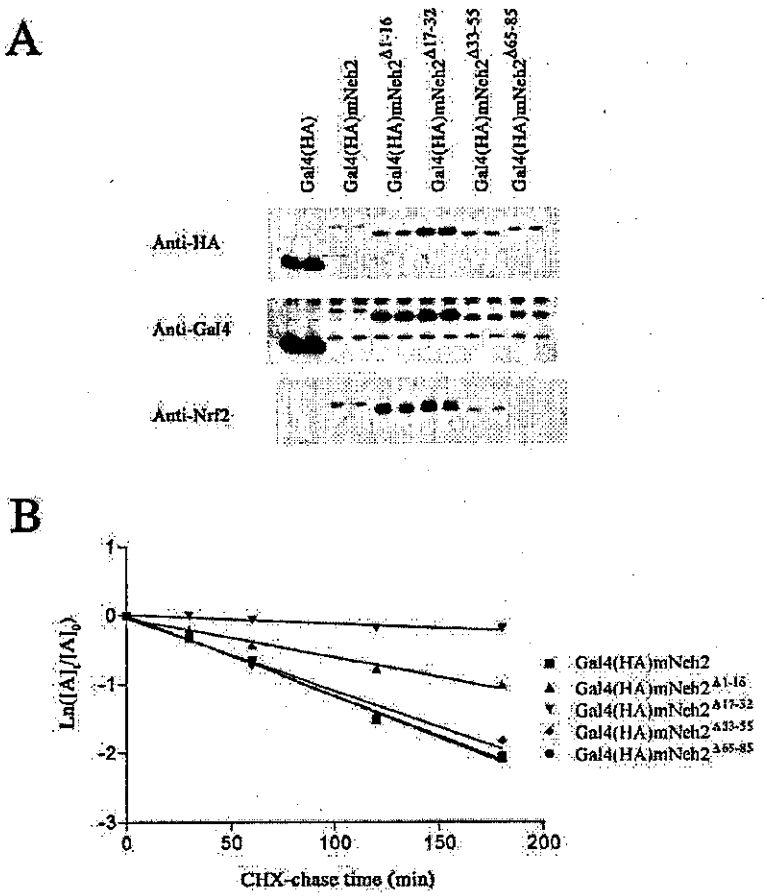

FIG. 2. **The DIDLID element is essential for Keap1-independent, Neh2-mediated degradation.** COS1 cells in 60-mm tissue culture dishes were transfected with 2 μg of a vector expressing either Gal4(HA), Gal4(HA)mNeh2, or various related deletion proteins as indicated in the figure. pcDNA3.1/mKeap1 (2 μg) was included in all transfection mixes as was 0.8 μg of pCMVβ-gal. *A*, whole-cell lysates were prepared from duplicate monolayers 24 h later, and the steady-state expression levels of the Gal4(HA) and related fusion proteins were determined by immunoblot analysis with the antibodies indicated to the *left* of each panel. *B*, CHX was spiked into each dish of cells to a final concentration of 40 μg/ml CHX. Subsequently, for each of the indicated fusion proteins, whole-cell lysates were prepared from transfected cells after the indicated CHX chase periods and probed with a mouse anti-HA antibody. The graph depicts the natural logarithm of the relative expression of each fusion protein (quantitated by densitometry) as a function of CHX chase time (mean of three independent experiments). The best fit line and the half-life, derived from the mean ± S.E. of the best-fit-line, are indicated for each fusion protein.

steady-state level achieved by the wild-type Neh2 fusion protein (data not shown). This is consistent with a prediction based on the magnitude of the increase in its half-life. Our interpretation of these experimental data is that both the wild-type and the DIDLID deletion fusion proteins are synthesized and fold correctly at the same rate. Therefore, at steady-state, both must be degraded at the same rate, and this explains the similarity in the absolute amount of these proteins found conjugated to ubiquitin. The increased total amount of fusion protein lacking Neh2 residues 17–32 arises because in the absence of the DIDLID element the rate of ubiquitination is reduced, and a greater cellular concentration of this fusion protein is required in order to achieve a similar cellular concentration of ubiquitinated material.

Given the fact that Gal4(HA)mNeh2$^{\Delta 1-16}$ is more stable than the wild-type fusion protein, we expected to find that its fractional ubiquitination was also less than that for Gal4(HA)mNeh2. Surprisingly, this does not appear to be the case (Fig. 3*A*, *cf. lanes 1* and *2* with *lanes 3* and *4*). By serial dilution, it was shown that the fractions of Gal4(HA)mNeh2 and Gal4(HA)mNeh2$^{\Delta 1-16}$ are essentially equivalent (supplemental Fig. 2). Furthermore, to check whether ubiquitination of Gal4(HA)mNeh2$^{\Delta 17-32}$ might be driven to some extent by the region of Neh2 encompassed by amino acids 1–16, we measured the fraction of Gal4(HA)mNeh2$^{\Delta 1-32}$ that was recovered conjugated to ubiquitin at steady state. The fraction of this protein that was ubiquitinated did not differ from the fraction measured for Gal4(HA)mNeh2$^{\Delta 17-32}$ (Fig. 3*B*, *cf. lanes 1* and *2* with *lanes 3* and *4*). Thus, deletion of amino acids 1–16 in Neh2 does not appear to compromise the capacity of the fusion protein to be ubiquitinated. The enhanced stability of the fusion protein attendant upon this deletion does not appear interpretable in terms of the conventional paradigm of proteasomal degradation. Perhaps, in some currently undefined fashion, this deletion affects not the rate of ubiquitination but rather the rate of degradation by the proteasome of the ubiquitinated substrate.

We also analyzed the fractional ubiquitination of Gal4(HA)mNeh2$^{\Delta 33-55}$, and it was identical to that of the wild-type fusion protein (data not shown). Unfortunately, although we can detect ubiquitinated fusion proteins with rabbit anti-Nrf2 serum, we cannot do so with the rabbit anti-Gal4 or mouse anti-HA reagents. We presume that ubiquitination occludes or modifies these regions of the fusion protein. As a consequence, this has precluded an analysis of the ubiquitin status of Gal4(HA) and Gal4(HA)mNeh2$^{\Delta 65-85}$.

The above results indicate that the DIDLID element in the Neh2 degron is necessary to allow efficient ubiquitination of Gal4(HA)mNeh2. Furthermore, the inverse correlation between the stabilities of Gal4(HA)mNeh2$^{\Delta 17-32}$ and Gal4(HA)mNeh2 and the extent to which they were ubiquitinated indicated that this type of modification was functionally important for Keap1-independent, Neh2-mediated proteasomal degradation. Nonetheless, the observation that a protein can be both proteasomally degraded and polyubiquitinated does not prove that a causal link exists between the two. For example, p21^{Cip1} is polyubiquitinated *in vivo* and is degraded by the proteasome, but mutants lacking lysine residues remain unstable (30). We therefore investigated whether polyubiquitination was necessary for degradation of Gal4(HA)mNeh2 by using the ts20TG^{R} cell line; these cells express a temperature-sensitive mutant E1 (ubiquitin-activating) enzyme, and at the nonpermissive temperature of 39 °C the enzyme is inactivated

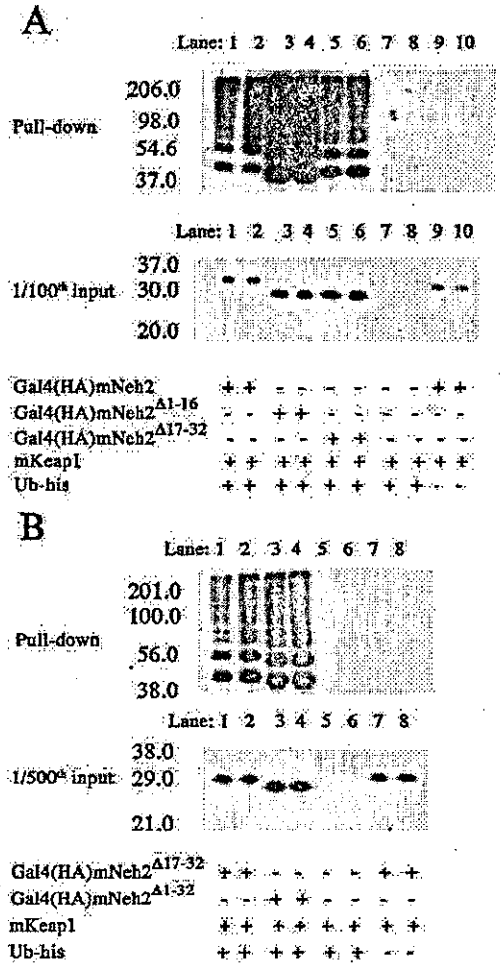

FIG. 3. **The DIDLID element directs polyubiquitination of Gal4(HA)mNeh2.** *A* and *B*, duplicate dishes of COS1 cells were transfected with the indicated plasmids. After transfection (24 h), a whole-cell lysate (input) and an affinity-purified His-tagged fraction (pull-down) were prepared from each dish of transfected cells and blotted with rabbit anti-mNrf2 serum. M_r markers are indicated to the *left* of each blot. *Ub*, ubiquitin.

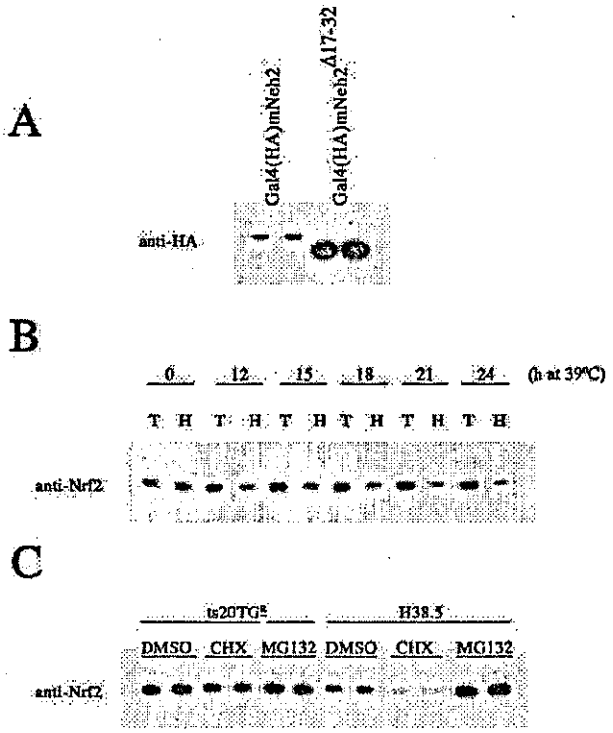

FIG. 4. **Polyubiquitination is essential for proteasomal degradation of Gal4(HA)mNeh2.** *A*, duplicate dishes of ts20TG^R cells were transfected with 2 μg of pcDNA3.1/mKeap1, 0.8 μg of pCMVβ-gal, and 2 μg of an expression vector for either Gal4(HA)mNeh2 or Gal4(HA)mNeh2$^{\Delta 17-32}$, as indicated. After transfection (24 h), whole-cell lysates were prepared from each dish of cells and probed with mouse anti-HA. *B* and *C*, dishes of either ts20TG^R (T) or H38.5 (H) cells were transfected with 2 μg of pcDNA3.1/mKeap1, 0.8 μg of pCMVβ-gal, and 2 μg of an expression vector for Gal4(HA)mNeh2. *B*, dishes of cells were maintained at 34.5 °C and shifted to the nonpermissive temperature of 39 °C at such times that approximately 40 h after transfection they had been exposed to the nonpermissive temperature for the indicated times. At this point, whole-cell lysates were prepared from each dish of cells and blotted with rabbit anti-mNrf2. *C*, ~16 h after transfection, all dishes were shifted to the nonpermissive temperature of 39 °C for 15 h. Subsequently, duplicate dishes were treated with either 0.1% (v/v) Me_2SO (*DMSO*, vehicle), 40 μg/ml CHX, or 10 μM MG132 for 3 h, before whole-cell lysates were prepared from each dish of cells and probed with rabbit anti-mNrf2.

resulting in failure to covalently attach ubiquitin to proteins. The modes of degradation of Gal4(HA)mNeh2 appear to be similar in ts20TG^R and COS1 cells as deletion of the DIDLID motif resulted in a large increase in the steady-state expression level of the fusion protein in both cell lines (*cf.* Fig. 2*A* and Fig. 4*A*). When Gal4(HA)mNeh2 was heterologously expressed in ts20TG^R cells, and then transferred to 39 °C, the fusion protein did accumulate, albeit by a modest 3-fold (Fig. 4*B*). Nonetheless, in the control cell line, H38.5, derived from the ts20TG^R cell line but expressing wild-type E1 enzyme which maintains some activity at 39 °C, the Gal4(HA)mNeh2 protein failed to increase upon transfer to the nonpermissive temperature (Fig. 4*B*). It is therefore concluded that a functional ubiquitin-conjugating system is essential for efficient proteasomal degradation of Gal4(HA)mNeh2.

Subsequent experiments indicated that the modest increase in the level of the fusion protein was likely to be a consequence of a nonproteasomal mode of degradation of the fusion protein in ts20TG^R cells maintained at 39 °C. To test this hypothesis, Gal4(HA)mNeh2 was heterologously expressed in both the ts20TG^R and the H38.5 cell lines. The two cell lines were shifted to 39 °C for 15 h, and duplicate dishes of cells were treated with either vehicle (Me_2SO), translation inhibitor CHX, or the proteasomal inhibitor MG132 for a further 3 h. In the ts20TG^R cell line, treatment with MG132 did not lead to any accumulation of Gal4(HA)mNeh2 beyond that of Me_2SO-treated cells, suggesting that the inactivation of E1 was complete and no proteasomal degradation of Gal4(HA)mNeh2 occurred in this cell line at 39 °C (Fig. 4*C*). In comparison, accumulation of the fusion protein was evident in H38.5 cells upon treatment with MG132 (Fig. 4*C*). Despite the absence of detectable proteasomal degradation of Gal4(HA)mNeh2 in ts20TG^R cells at 39 °C, the 3-h CHX chase clearly resulted in a diminution in the amount of the protein. We attribute this to an unidentified, nonproteasomal degradation pathway.

The data presented above demonstrate that ubiquitination is essential for Keap1-independent, Neh2-mediated proteasomal degradation and that its DIDLID element is critical to ensure efficient ubiquitination.

Both the DIDLID Element and the ETGE Motif in Neh2 Are Essential to Confer Redox Sensitivity and Keap1 Dependence Upon the Half-life of Nrf2—Deletion of the DIDLID element from the Neh2 domain does not affect its capacity to interact with Keap1 because, by coimmunoprecipitation assay, we could

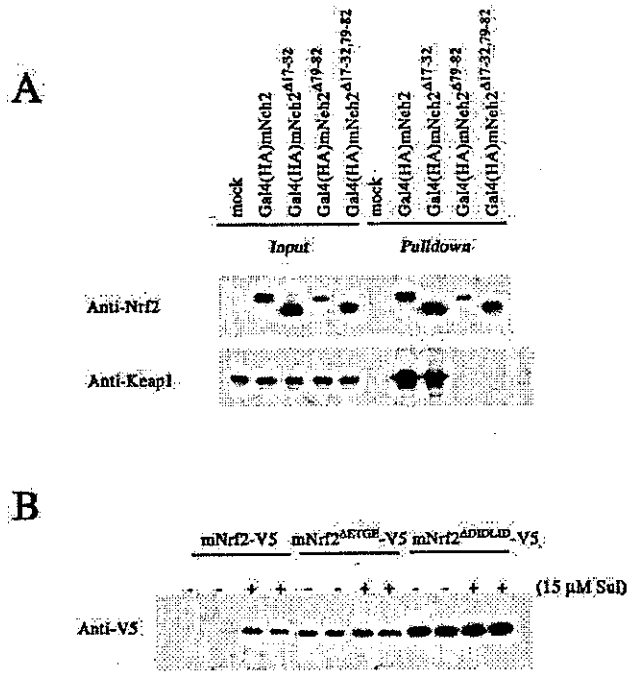

FIG. 5. **The DIDLID element does not influence the interaction of Nrf2 with Keap1.** *A*, COS1 cells in 60-mm dishes were either mock-transfected or transfected with vectors expressing the indicated fusion proteins, and 24 h later whole-cell lysates were prepared. To each of these lysates was added an equal volume of lysate from COS1 cells transfected with pcDNA3.1/V5HisCmKeap1. A portion of the lysate was kept as an input sample. HA-tagged material was immunoprecipitated from the remaining portion of each lysate. Both these *pull-down* fractions and *input* samples were probed by immunoblot with either rabbit anti-mNrf2, to detect the Neh2-fusion proteins, or with goat anti-hKeap1 to detect mKeap1-V5-hexahistidine. *B*, COS1 cells in 60-mm dishes were transfected with 2 μg of pcDNA3.1/mKeap1, 0.8 μg of pCMVβ-gal, and 2 μg of vector expressing either mNrf2-V5, mNrf2$^{\Delta ETGE}$-V5, or mNrf2$^{\Delta DIDLID}$-V5. 24 h after transfection, duplicate dishes of cells were treated with either 0.1% (v/v) Me_2SO (−) or 15 μM Sul (+) for 1 h, at which point whole-cell lysates were prepared and probed with mouse anti-V5 by immunoblot.

demonstrate that Gal4(HA)mNeh2$^{\Delta 17-32}$ can interact with mKeap1 in cell lysates (Fig. 5*A*). It was therefore possible to determine whether Keap1 required not only the ETGE motif in Neh2 but also the DIDLID element in order for it to destabilize Nrf2 in homeostatic cells.

We coexpressed mNrf2$^{\Delta DIDLID}$-V5 (mNrf2 lacking amino acids 17–32 and tagged at the C terminus with the V5 epitope) with untagged mKeap1 in COS1 cells, which were subsequently treated with vehicle or Sul for 1 h before preparing whole-cell lysates. The level of mNrf2$^{\Delta DIDLID}$-V5 expressed at steady-state was invariant between the homeostatic and stressed cells (Fig. 5*B*), suggesting that the DIDLID element is essential for Keap1 to enhance the turnover rate of Nrf2 in homeostatic cells and, by implication, that Keap1 functions as part of the same pathway operative for Keap1-independent, Neh2-mediated degradation. Under the same conditions, mNrf2-V5 was expressed at lower levels in homeostatic cells than in stressed cells, and as expected, this was Keap1-dependent as deletion of the ETGE motif, to generate mNrf2$^{\Delta ETGE}$-V5, resulted in a protein whose expression level was elevated compared with its wild-type counterpart in homeostatic cells; its expression level was not affected by treatment with Sul.

To verify that Keap1 cannot enhance the turnover of mNrf2$^{\Delta DIDLID}$-V5 in COS1 cells, we determined its half-life in the presence and absence of heterologous mKeap1, both under homeostatic conditions and in cells that had been treated with Sul for 2 h (Fig. 6, *E* and *F*). It is evident that the half-life of this protein was similar under all conditions tested. In particular, when coexpressed with mKeap1, mNrf2$^{\Delta DIDLID}$-V5 had a half-life in homeostatic COS1 cells of 38 min and a half-life of 41 min in cells pretreated with Sul for 2 h (Fig. 6*F*).

As expected, the half-life of mNrf2$^{\Delta ETGE}$-V5 was also independent of whether mKeap1 was coexpressed or absent and whether the cells were homeostatic or stressed. This protein had a half-life of ~30 min under all tested conditions (Fig. 6, *C* and *D*).

Keap1 was only able to destabilize mNrf2-V5 protein containing both the ETGE motif and the DIDLID element in homeostatic COS1 cells. In stressed COS1 cells heterologously expressing mNrf2-V5 only, the half-life of the bZIP protein was 30 min, statistically indistinguishable from that of mNrf2$^{\Delta ETGE}$-V5 (Fig. 6, *A* and *C*). In homeostatic COS1 cells, however, the half-life of mNrf2-V5 was only 24 min (Fig. 6*A*). The reduced stability of mNrf2-V5, in the absence of heterologous mKeap1, in homeostatic COS1 cells is in agreement with our previous observation that the level of expression of tagged mNrf2 is enhanced by oxidative stress, even in the absence of heterologous mKeap1 (Ref. 15, Fig. 5*B*). It presumably reflects the presence of endogenous Keap1 in COS1 cells. Coexpression of mKeap1 with mNrf2-V5 further reduced the stability of the transcription factor in homeostatic cells. Under these conditions, mNrf2-V5 had a half-life of <7 min in homeostatic cells and a half-life of 38 min in stressed cells (Fig. 6*B*).

Two aspects of the data in Fig. 6 warrant further comment. First, the degradation of mNrf2-V5, when coexpressed with mKeap1, in homeostatic COS1 cells does not follow first-order kinetics. The quoted half-life was determined from an approximation of the initial rate of degradation at $t = 0$ min. As we could not model the curve using any common mathematical function, an initial "half-life" of 7 min was estimated from the slope of a line through the $t = 0$ and $t = 15$ min data points. A potential explanation for the observed kinetics of degradation is offered under "Discussion."

Second, the data suggest that not only does mKeap1 destabilize mNrf2-V5 in homeostatic COS1 cells, it might actually stabilize mNrf2-V5 in stressed cells. Thus, mNrf2-V5 expressed in stressed COS1 cells that lack heterologous mKeap1 has a half-life of 30 min. However, when mKeap1 is coexpressed with mNrf2-V5 in such cells, the half-life of the bZIP protein rises to 38 min (Fig. 6, *A* and *B*). No corresponding enhancement in half-life is observable for the mutant protein mNrf2$^{\Delta ETGE}$-V5 (Fig. 6, *C* and *D*). This effect of mKeap1 on the stability of mNrf2-V5 in stressed cells was found to be reproducible, although it is modest. This observation may not be of broad physiological relevance but may be related to limitations of the model system being investigated.

Collectively, these data support a model in which Keap1 destabilizes Nrf2 in homeostatic cells by directly interacting with the transcription factor through the ETGE motif, and thereby enhancing the rate of degradation mediated by the DIDLID element. Taken with our previous observation that mKeap1 does not influence the ubiquitination status of mNrf2-V5 under conditions where it does reduce its half-life (15), this suggests that Keap1 enhances the rate of Neh2-mediated degradation in homeostatic COS1 cells by acting downstream of ubiquitination mediated by the DIDLID element.

The Neh6 Domain Is a Redox-insensitive Degron, Which Is Essential for Degradation of mNrf2 in Oxidatively Stressed Cells—The fact that deletion of the DIDLID element only increased the half-life of mNrf2-V5 ~6-fold (from <7 min to ≈40 min) was unexpected because deletion of this region from Gal4(HA)mNeh2 resulted in a fusion protein that was almost

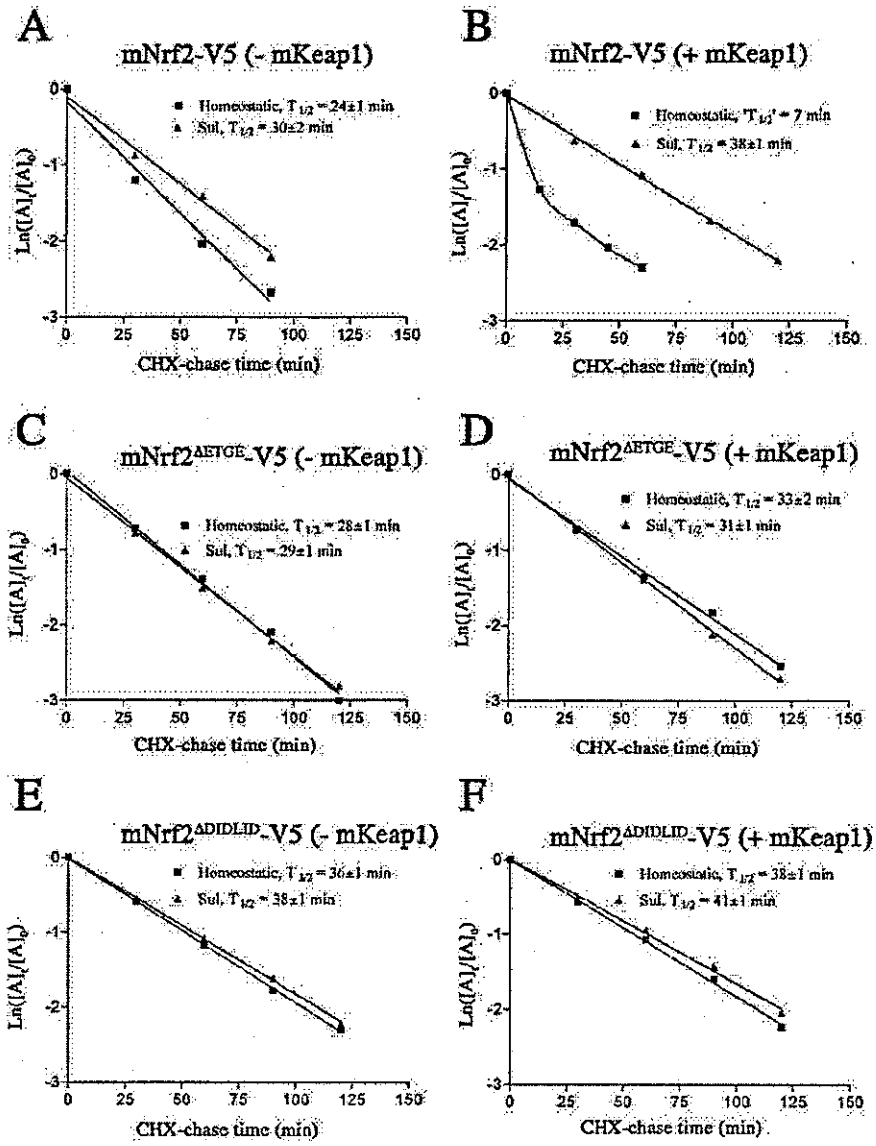

FIG. 6. **Both the DIDLID and the ETGE motifs of Nrf2 are essential to confer redox sensitivity upon Nrf2.** COS1 cells in 60-mm dishes were transfected with 2 μg of vector expressing either mNrf2-V5, mNrf2$^{\Delta ETGE}$-V5, or mNrf2$^{\Delta DIDLID}$-V5. Cells were cotransfected with 2 μg of either empty vector (*−mKeap1*) or vector expressing untagged mKeap1 (*+mKeap1*). pCMVβ-gal was included in all transfection mixes (0.8 μg) as an internal control. This gave six populations of cells differing in the proteins that they heterologously expressed (*A–F*). 24 h after transfection, cells were treated with either 0.1% (v/v) Me_2SO (homeostatic) or 15 μM Sul for 2 h before CHX was spiked into each dish to a final concentration of 40 μg/ml. Subsequently, whole-cell lysates were prepared at different time points and probed with mouse anti-V5. Each graph depicts the natural logarithm of the relative expression of V5-tagged protein as a function of CHX chase time in both homeostatic and stressed COS1 cells (mean of between two to four independent experiments). The best fit line and half-life, derived from the mean ± S.E. of the slope of the best fit line, are presented.

completely stable in COS1 cells. Furthermore, deletion of essentially the entire Neh2 domain from mNrf2-V5, to generate mNrf2$^{\Delta 3-85}$-V5, yielded a protein that had a half-life of only 37 min (Fig. 7*A*). These results suggested that Neh2 is not the sole degron in mNrf2, and two further points were evident. First, the second degron(s) was redox-insensitive as the half-life of mNrf2$^{\Delta DIDLID}$-V5 was not altered by treatment of COS1 cells with Sul (Fig. 6, *cf. E* and *F*). Second, the sole presence of the second degron(s) was sufficient to dictate the turnover rate of the transcription factor in oxidatively stressed COS1 cells. Thus while the Neh2 degron confers instability on the protein in homeostatic cells, it could be inactivated without impacting on the half-life of the protein in stressed cells. For example, mNrf2-V5, coexpressed with mKeap1 in stressed COS1 cells, had a half-life of 38 min, nearly identical to the half-life of mNrf2$^{\Delta DIDLID}$-V5 under similar conditions (Fig. 6, *cf. B* with *F*).

To delineate the region of Nrf2 required for its instability in stressed cells, we initially focused on Neh4 and Neh5 (amino acids 116–131 and 177–193, respectively, see supplemental Fig. 1) because they have been reported as transactivation domains (31), and such regions are occasionally coincident with degrons (23). To investigate Neh4 and Neh5, constructs expressing mNrf2$^{\Delta DIDLID,\Delta 116-131}$-V5 and mNrf2$^{\Delta DIDLID,\Delta 177-193}$-V5 were generated. Furthermore, the Neh6 domain was examined similarly, because it is a region of the protein that has had no function ascribed to it to date. As two particular regions within the Neh6 domain